ISTANBUL TECHNICAL UNIVERSITY ★ GRADUATE SCHOOL OF SCIENCE ENGINEERING AND TECHNOLOGY

DIRECT SCATTERING PROBLEM FOR 3-D INHOMOGENEOUS MATERIALS LOADED INSIDE CIRCULAR WAVEGUIDE

M.Sc. THESIS

Ahmet AYDOĞAN

Department of Electronics and Communication Engineering

Telecommunication Engineering Programme

JUNE 2012

ISTANBUL TECHNICAL UNIVERSITY ★ GRADUATE SCHOOL OF SCIENCE ENGINEERING AND TECHNOLOGY

DIRECT SCATTERING PROBLEM FOR 3-D INHOMOGENEOUS MATERIALS LOADED INSIDE CIRCULAR WAVEGUIDE

M.Sc. THESIS

Ahmet AYDOĞAN
(504091347)

Department of Electronic and Communication Engineering

Telecommunication Engineering Programme

Thesis Advisor: Assoc. Prof. Dr. Funda AKLEMAN

JUNE 2012

İSTANBUL TEKNİK ÜNİVERSİTESİ ★ FEN BİLİMLERİ ENSTİTÜSÜ

DAİRESEL DALGA KILAVUZUNA YERLEŞTİRİLMİŞ ÜÇ BOYUTLU HOMOJEN OLMAYAN CİSİMLER İÇİN DÜZ PROBLEMİN ÇÖZÜMÜ

YÜKSEK LİSANS TEZİ

Ahmet AYDOĞAN
(504091347)

Elektronik ve Haberleşme Mühendisliği Anabilim Dalı

Telekomünikasyon Mühendisliği Programı

Tez Danışmanı: Doç. Dr. Funda AKLEMAN

HAZİRAN 2012

Ahmet Aydoğan, a **M.Sc** student of ITU **Graduate School of Science** student ID **504091347**, successfully defended the **thesis** entitled "**DIRECT SCATTERING PROBLEM FOR 3-D INHOMOGENEOUS MATERIALS LOADED INSIDE CIRCULAR WAVEGUIDE**", which he prepared after fulfilling the requirements specified in the associated legislations, before the jury whose signatures are below.

Thesis Advisor :	**Assoc. Prof. Dr. Funda AKLEMAN** Istanbul Technical University	....
Jury Members :	**Assoc. Prof. Dr. Cevdet IŞIK** Istanbul Technical University	....
	Prof. Dr. Ercan TOPUZ Doğuş University	....

Date of Submission : 4 May 2012
Date of Defense : 7 June 2012

To everyone, who stood by me during this period,

FOREWORD

First and foremost I offer my sincerest gratitude to my supervisor Associate Professor Doctor Funda Akleman. She never hesitated to give me support and encouragement. Without her efforts, this thesis would not be a success.

I also want to thank Professor Doctor Ali Yapar, of being great help during the development of this thesis and for being role model that will always guide me through my academic career.

I would also like to thank Professor Doctor Ercan Topuz and Professor Doctor Levent Sevgi for their support whenever I need.

Finally; I would like to thank TUBITAK (the Scientific and Technological Research Council of Turkey) for supporting me financially by the project 108E146.

May 2012

Ahmet AYDOĞAN
Telecommunication Engineer

TABLE OF CONTENTS

Page

ABBREVIATIONS

DGF **:** Dyadic Green's Function
HFSS **:** High Frequency Structure Simulator
MoM **:** Method of Moments
MMM **:** Mode Matching Method
PCTD **:** Pie Cell Type Division
RCTD **:** Rectangular Cell Type Division

LIST OF FIGURES

DIRECT SCATTERING PROBLEM FOR 3-D INHOMOGENEOUS MATERIALS LOADED INSIDE CIRCULAR WAVEGUIDE

SUMMARY

In this study, a scattering analysis for a partially loaded circular cross section waveguide, which is required for the solution of inverse problem, is realized. The inverse scattering problem considered here can be used for the determination of constitutive parameters of a lossy dielectric or for the design of a required filter characteristics, where the incident field is known and scattered field is measured. In order to show the validity of this approach, it is first required to solve the direct scattering problem using a dyadic Green's function representation of the electromagnetic fields for circular cross-section waveguide. Then, the similar representation can be used for the inverse algorithm.

In direct scattering problem, the incident field and the constitutive parameters of the (relative permittivity, relative permeability, conductivity) material are known and the scattered field, generated by the volume current density inside the object is aimed to be determined. In this study, a non-magnetic, lossy dielectric and partially loaded three-dimensional material, loaded inside a circular waveguide is examined. Due to the complexity of the problem, instead of analytical techniques, numerical methods are used. The proposed numerical technique is Method of Moments (MoM). Implementing this method, two different cell types are offered. First cell type, used in Method of Moments procedure is rectangular where the dyadic Green's function elements in the source region do not converge with this type cell division. Since the number of modes generated by the volume current density inside the object is not known, rectangular cell type is not suitable for most of the problems including arbitrarily shaped or inhomogeneous lossy dielectric objects loaded in a circular waveguide. Therefore, rectangular cells can only be utilized for the problems where the number of modes, excited by the object, is less than the convergence limit. For instance, a cross-section filled, lossless material, excited by dominant mode, only produces only the dominant mode.

To overcome the divergency problem, which is encountered when rectangular type cell is used, another cell type is proposed and analyzed. Pie cell type division converge in the source region and is convenient for multi-mode problem. Optimization of this division is analyzed and results are given with examples. It is shown that a cell with equal increments, both in ρ and ϕ directions gives better results. In order not to increase the computational cost, cell dimensions are mostly chosen around $\lambda/25$. It is shown that, equal cell size in all directions, gives better accuracies.

The results for fully loaded materials are compared with Mode Matching Method (MMM) and the commercial software High Frequency Structure Simulator (HFSS). Comparison is done between amplitudes and phases of scattering parameters. Since circular waveguide is a two port structure, S_{11} and S_{21} are used for comparisons.

Numerical examples are given for fully and partially loaded materials, where both Mode matching Method (MMM) is used as the reference solution for fully loaded problems while only HFSS is used as the reference solution of partially loaded waveguides. It should be noted that, HFSS solution for fully loaded case is also calibrated using the results obtained via MM. Examples are also carried out with conductivity of material is greater than zero. Comparing MoM, HFSS and MMM, validity is proved for the direct scattering problem in circular waveguide.

Evaluation of dyadic Green's function for circular waveguide by direct scattering problem, provides a basis for inverse algorithm for reconstructing the complex permittivity of three-dimensional, inhomogeneous and arbitrarily shaped objects, loaded in circular waveguide.

DAİRESEL DALGA KILAVUZUNA YERLEŞTİRİLMİŞ ÜÇ BOYUTLU HOMOJEN OLMAYAN KAYIPLI CİSİMLER İÇİN DÜZ PROBLEMİN ÇÖZÜMÜ

ÖZET

Bu çalışmada, dairesel dalga kılavuzuna ilişkin ters saçılma probleminin çözümü için temel oluşturmak hedeflenmiştir. Ters saçılma problemi, bir malzemenin iletkenlik, dielektrik sabiti gibi elektriksel özelliklerinin belirlenmesini ele alan bir yöntemdir. Ters saçılma probleminde uygulanan elektromanyetik dalga belirlidir. Dalganın yayılma yönünde cisimden dolayı oluşan süreksizlikten kaynaklanan saçılan alan bilgisi de bilinmektedir. Bu iki bilgi ile süreksizliğin elektriksel özellikleri bulunabilir. Elde edilen bilgiler fiziksel olarak, gerektiği taktirde aynı zamanda cismin şekli ve konumu ile ilgili bilgiyi de verecektir.

Ters saçılma probleminin çözümü için problemin doğasına ilişkin olarak farklı yöntemler uygulanabilir. Problem açık veya kapalı alanda ele alınabilir. Dalga kılavuzu yöntemi bu yöntemlerden biridir. Burada dalga kılavuzu yöntemi ile ters problemin çözümüne ilişkin altyapı oluşturulmuştur. Dalga kılavuzu olarak dairesel dalga kılavuzu seçilmiştir. Ters problemin çözülebilmesi için verilen yapıya ilişkin dyadik Green fonksiyonunun geçerliliğinin kontrol edilmesi gerekmektedir. Bu tür bir değerlendirme dairesel dalga kılavuzuna ilişkin düz problemin çözümü ile yapılabilir. Düz saçılma probleminde uygulanan elektromanyetik dalga bilgisi ile birlikte dalganın yayılma bölgesinde süreksizliğe neden olan cismin konumu, şekli ve elektriksel özellikleri bilinmektedir. Aydınlatılan cisimde oluşan eşdeğer akım yoğunluğu saçılan elektrik alan oluşmasına neden olacaktır. Oluşan saçılan elektrik alanın incelenen bölgenin herhangi bir noktasında belirlenmesi düz problemin amacını oluşturmaktadır.

Hem ters saçılma problemine ilişkin temel oluşturması açısından, hem de literatürde, bildiğimiz kadarı ile konuya ilişkin bir çalışma olmaması nedeniyle daire kesitli dalga kılavuzuna kısmi olarak yerleştirilmiş, manyetik olmayan, kayıplı yalıtkan malzemeler için düz saçılma problemin çözümü bu çalışmanın amacını oluşturmuştur.

Uyarılan alandan dolayı dielektrik cisim içinde polarizasyon akımı indüklenecektir. İndüklenen bu akımdan dolayı saçılan alan oluşacaktır. Gelen alan, toplam alan ve saçılan alan arasındaki bağıntılar problemin çözümü için ilişkilendirilmiştir. Uzayın herhangi bir noktasındaki toplam alan, o noktadaki gelen alan ile saçılan alanın toplamı cinsinden ifade edilmiştir. Ayrıca hacim eşdeğer teoremi ile cisim içindeki toplam alan ile indüklenen akım arasında bağıntı kurulmuştur. Tüm bu ilişkiler integral denklemleri ile ifade edilmiş ve denklem sistemi dyadik Green fonksiyonları entegre edildikten sonra indüklenen akım ile gelen alan arasındaki ilişkiye indirgenmiştir. Bu ilişkide indüklenen akım bilinmeyendir ve gelen elektrik alan bilgisi bilinmektedir.

Ele alınan problemin karmaşıklığından dolayı analitik çözümler yetersiz kalmaktadır. Bu nedenle problemin çözümü için bilgisayar destekli sayısal yöntem kullanılmıştır. Problemin çözümüne ilişkin elde edilen denklemler integral denklem biçiminde olduğundan kullanılan sayısal yöntem olarak Moment yöntemi önerilmiştir. Moment yönteminde, çözüme ilişkin integral denklemi, baz fonksiyonları ve ağırlık fonksiyonları kullanılarak bir dizi lineer denklem cinsinden ifade edilir. Lineer denklemler düzenlenerek matris denklemlerine dönüştürülür. Bulunmak istenen büyüklükler matris denklemlerinin çözümü ile elde edilir.

Moment yöntemi uygulanırken incelenen bölge hücrelere bölünmüştür. Baz fonksiyonu olarak dürtü fonksiyonu seçilmiştir. Her hücre içinde polarize akımın düzgün dağıldığı varsayılmıştır ve sayısal açıdan bakacak olursak herhangi bir hücredeki akım değerinin başka bir hücreyi etkilemediği varsayımı yapılmıştır. Örneğin sinc fonksiyonu veya üçgen biçiminde bir baz fonksiyonu seçilirse matematiksel olarak herhangi bir hücredeki akımın diğer hücrelerdeki akıma da katkı yapacağı varsayılmış olacaktır. Bu tür baz fonksiyonları daha tutarlı sonuç verme yeterliliğine sahipse de, modellemenin zorluğu ve hesaplamaların ağırlaşması nedeni ile baz fonksiyonu olarak dürtü fonksiyonu seçilmesine karar verilmiştir.

Green fonksiyonu doğası gereği kaynak ve gözlem noktası aynı olduğu durum için tekillik içermektedir. Bu tekillik sorununu çözmek için kaynak ve gözlemin aynı olduğu durumda kaynağın bulunduğu yerin etrafında çok küçük hacimli bir bölgenin integral hesabına katılmaması uygulanan bir yöntemdir. Bu yöntem asal hacim *(principle volume)* yöntemi olarak adlandırılır. Asal hacim olarak adlandırılan bu ifade ayrıca integral denklemine eklenir. Kaynak ve gözlem noktasının üst üste geldiği küçük hacmin integral katkısını veren bu ifade tamamen çıkarılan bölgenin geometric yapısına bağlıdır. Bu çalışmada iki tip hücre dağılımı önerilmiştir. Her iki hücre tipi için de kaynak ve gözlemin aynı olduğu durumlarda çıkarılan bölge z yönünde sonsuz küçük kalınlıkta bir kesit olarak kabul edilmiştir. Bu çıkarılan bölgeye denk düşen kaynak dyadik ifadesi $\hat{e}_z \times \hat{e}_z$ problemin çözümüne ilişkin integral denklemine dahil edilmiştir.

Sayısal yöntem kullanılarak problem ele alındığı için hücrelendirme yapmak gerekmektedir. Bu çalışmada önerilen birinci tip hücre dağılımı dikdörtgen yapıda, ikinci tip hücre dağılımı dart yapıdadır. İlk ele alınan dikdörtgen hücre yapısı geometrik olarak kartezyen koordinatlarda ifade edilmektedir. Dairesel dalga kılavuzuna ait dyadik Green fonksiyonu bileşenleri silindirik koordinat sisteminde tanımlanmış olduğundan dikdörtgen hücrelemede yalnızca kaynak hücresinin konumunu belirten r' vektörünün z bileşenini içeren dyadik Green fonksiyonu elemanlarının integralleri analitik olarak gerçeklenmiştir. Diğer bileşenleri içeren terimler ise hücre içinde sabit etkide bulunduğu kabul edilip, hücrenin ρ ve ϕ yönlerinde oluşan yüzeyin alanı ile çarpılarak değerleri hesaplanmıştır. Bu tip hücrelendirme sayısal hesap yükünü azaltmaktadır. Dikdörtgen hücre tipi için dyadik Green fonksiyonu kaynak noktasında hesaplanmak istendiğinde matematiksel ifadesindeki sonsuz seri toplamı belli bir değerde kesildiği zaman Green fonksiyonunun integraline ilişkin matrisin köşegen elemanlarının yakınsamadığı görülmüştür. Bu tip hücrelendirme sayısal yük açısından bahsedilen avantajına rağmen kaynak noktasında böyle bir sıkıntı oluşturmaktadır. Tam dolu ve kayıpsız malzemeler için cisim içinde oluşan modlar uyarılan alanın modları ile sınırlı olduğu için bu durumda yakınsama olmaması bir sıkıntı oluşturmamaktadır. Ayrıca problem gereği yüksek modların etkisinin ortaya çıkmadığı durumlarda yine dikdörtgen hücrelendirme çözüm için yeterli olmuştur. Ancak daha genel bir çözüm üretebilmek için ikinci bir tip hücrelendirme önerilmiştir. Hücre tip ρ,ϕ ve z yönlerinde tanımlı ve dikdörtgen hücre tipinin aksine kaynağı temsil eden dyadik Green fonksiyonlarının tümünün integralinin analitik olarak elde edildiği dart tipidir. Bu tip hücrelendirmenin, sayısal yükü arttırmasına rağmen dyadik Green fonksiyonunun hesabı için çıkılan üst modlarda yakınsadığı görülmüştür. Bu nedenle dart bölmelendirmenin genel çözüm için uygun olduğu kanısına varılmıştır. Dart hücrelendirme için sayısal hesaplama yükü ve elde edilen sonuçların tutarlılığı açısından en iyileme incelemeleri yapılmıştır. Hücrenin tüm yönlerdeki boyutlarının birbrilerine yakın tutulmasının sonuçları iyileştirildiği görülmüştür. Ayrıca kesitin merkezini çevreleyen bölgede bulunan hücre sayısının arttırılması sonuçları iyileştirmiştir. Burada varılan kanı, sinüzoidal fonksiyonların etkilerinin açıya bağımlılığından dolayı, ϕ yönünde daha hassas bir hücrelendirmenin tutarlı sonuçlara ulaşmak açısından önemli olmasıdır. Bilgisayar yeterliliğinden dolayı her yönde $\lambda/25$ boyutuna kadar inilebilmiştir. Bu durumda hatanın %1 civarlarında olduğu görülmüştür. Ele alınan başka bir örnekte cismin kalınlığı azaltılarak z yönünde $\lambda/45$ civarında bir hücre boyutu oluşturulmuş ve z yönünde üç katmanlı yapı için hatanın %0.15'e kadar azaldığı görülmüştür.

Bu çalışmada moment yöntemi ile elde edilen sonuçlar hem Mod Eşleştirme Yöntemi ile hem de ticari bir elektromanyetik benzetim programı olan HFSS ile karşılaştırılmıştır. Tam dolu ve elektriksel parametreleri en fazla z yönünün işlevi olan cisimler için karşılaştırma olarak Mod Eşleştirme Yöntemi referans olarak alınmıştır. Mod Eşleştirme Yöntemi dalga kılavuzunun içerisindeki süreksizlik durumlarında, sınır koşullarının kullanıdığı bir yöntemdir. Süreksizliğin her iki tarafında alanların modal açılımı yapılır. Modal fonksiyonlar elde edildikten sonra, problem her bölgedeki alan açılımlarıyla ilişkili modal katsayılarının belirlenmesine dönüşür. Normal modlar arasındaki diklik koşulu göz önüne alınarak bilinmeyen modal katsayılara ilişkin sonlu sayıda doğrusal denklemler elde edilir. Mod Eşleştirme Yöntemi ve Moment Metodu arasındaki karşılaştırma ve tutarlılık sayısal örnekler ile gösterilmiştir. Tam dolu, homojen olmayan, hem kayıplı, hem kayıpsız cisimler için elde edilen sonuçlar gayet olumlu olmuştur. Kısmen doldurulmuş cisimler için ise Mod Eşleştirme Yöntemi kullanılamamıştır. Bu durum için HFSS ile karşılaştırılma yapılmıştır. Ancak HFSS ile çalışılırken bazı sıkıntılarla karşılaşılmıştır. HFSS, dalga kılavuzunun açık uçlu modellenebilmesi için uygun sonlandırma gerektirmektedir ve bu durum S_{21} değerinin hesaplanmasını mümkün kılmamaktadır. Ayrıca HFSS programının dairesel cisimlerin benzetimi ve incelenmesi konusundaki yetersizliği sıkıntı oluşturmuştur.

Sonuç olarak bu çalışma ile birlikte dalga kılavuzu yöntemi kullanılarak dairesel dalga kılavuzu içine yerleştirilmiş kayıplı dielektrik cisimler için düz problem ele alınmıştır. Bu çalışma ile daire kesitli dalga kılavuzuna kayıplı, yalıtkan cisimlerin yerleştirilmeleri durumunda iki kapılı kılavuz yapısına ilşkin S parametreleri elde edilebilir. Ayrıca yalıtkan cisimin oluşturduğu süreksizlikten meydana gelen saçılan alanın ve toplam alanın kılavuz içinde herhangi bir noktadaki değeri bulunabilir. Herhangi bir kesitte veya çizgi üzerindeki toplam veya saçılan alanlar elde edilebilir. Aynı zamanda bu çalışma ile boş daire kesitli dalga kılavuzuna ait dyadic Green fonksiyonu ifadelerinin sağlaması yapılmıştır ve kılavuz içine yerleştirilen cismin elektriksel parametrelerinin belirlenmesini ele alan ters saçılma problem için de temel hazırlanmıştır.

1. INTRODUCTION

Scattering theory deals with the behavior of waves in case of being effected by obstacles or inhomogeneities in the propagating medium. More than a century, researchers increasingly investigate scattering problems. Developments in this area made scattering problems an important issue of electromagnetic theory.

Scattering problems, in electromagnetic theory, are investigated under two sub-groups; direct scattering problem and inverse scattering problem. Direct scattering problem deals with the determination of the scattered field caused by a discontinuity on the travelling axis of the incident electric field. In this problem, the incident electric field and the parameters of the object, causing discontinuity, such as the shape, location and electromagnetic parameters (magnetic permeability, permittivity, and conductivity) are assumed to be known.

There are several examples for analytical solution of direct scattering type problems in open literature. For instance, in [1], an analytical formulation for the direct scattering problem of one-dimensional, inhomogeneous anisotropic medium is handled. Closed form solutions of the scattered field are easily obtained using the boundary conditions on the interface between free space and anisotropic medium.

A study in geoscience, dealt with electromagnetic scattering theory and analysis of electromagnetic scattering characteristics of sea ice is presented in [2]. Multilayer random model for sea ice, including brine, air, snow, sea ice and pure ice is idealized as having plain interfaces and the direct scattering problem for the Helmholtz equation is formulated as a one-dimensional problem.

Analytical solutions are preferred if available for canonical problems. For direct scattering problem, another example for analytic solution is given in [3]. In mentioned study, the reflection and transmission coefficients are computed for radio-waves propagating through a dielectric slab. The permittivity in slab is decreasing symmetrically with an inverse-square profile, as to the middle axis up to the slab interfaces.

It is not easy to obtain exact analytical solutions and therefore numerical techniques are required for many type of scattering problems, which include complex geometries and inhomogenities. In [4], the reflection and transmission from an inhomogeneous slab is considered, where a finite difference approximation technique based on integral equation of the problem is developed for solving the direct scattering problem of an inhomogeneous slab.

The other branch of scattering problems, the inverse scattering problem is formulated to determine the location, shape and constitutive parameters of the object. In this problem, the scattered field is measured and the incident field is assumed to be known. To propose a solution for this type problem, the evaluation of DGF should be realized. This kind of evaluation is available by solution of direct scattering problem. Hence, the solution of direct scattering problem is the aim of this study.

Determination of electrical parameters of inhomogeneous materials is an important topic of electromagnetic theory and microwave theory due to its wide range of applications. Material test and measurements, fabrication and characterisation of multilayered structures, non-destructive testing and biomedical applications are some examples of this area. Inverse scattering problems examine the determination of materials. To solve this kind of problems, several methods are studied in closed, semi-open and open regions in literature. These methods have trade-offs due to the problem description. For instance, materials with wide dimensions and plate shaped are more suitable to be analyzed with free-space methods. Scattered fields from the corners and edges are to be inconsiderable. Some examples for free-space methods for direct and inverse scattering in the literature are listed as [5-7]. Cavity resonator method offers a high-accuracy solution but allows a narrow-band analysis. Implementing a wide-range of frequency analysis requires a collaboration of a few types of resonators, each allowing different frequency bands. Besides, waveguide methods provide wide range of frequency analysis and are opted chiefly for microwave applications.

In this study, direct scattering problem is handled by waveguide method for circular waveguide. In open literature, direct problem is analyzed for rectangular waveguide in [9]. Also, an analysis of scattering by metal objects in circular waveguide is valid [10]. In mentioned study, the discontinuity, inside the waveguide is PEC and scattered field is equal to the incident field. In addition, the object is a two-dimensional structure, hence formulation for dyadic Green's function (DGF) is integrated over surface integral variable.

To our knowledge, no existing research addresses the direct scattering problem for three dimensional, lossy dielectric objects, partially loaded in circular waveguide.

1.1 Purpose of Thesis

The main aim of this study is to prepare a basis for solution of inverse scattering problem in circular waveguide. Solving the inverse scattering problem, the determination of material can be realized. Determination includes the electrical properties of material as well as its shape and location, if required.

For determination of material, an integral equation technique for complex permittivity is introduced [11]. In that study, permittivity is only a function of longitudinal axes, hence material is fully loaded inside the rectangular waveguide. Then, imaging of inhomogeneous 3-D complex permittivity of arbitrary shaped materials loaded in a rectangular waveguide is presented in [12] and the numerical results are tested against real data by real measurement setup. The validity of method is proved. Mentioned studies dealt with the inverse problem in rectangular waveguide and gave satisfactory results.

We want to show that similar approaches are valid for different type of geometries. In this study, we had chosen circular waveguide. Before analyzing inverse scattering, one should realize the evaluation of dyadic Green's function for the given geometry.

In open literature, to the best of our knowledge, a solution of direct scattering problem for inhomogenous, lossy dielectric materials, partially loaded inside circular waveguide, does not exist. Due to the complexity of the problem and no existing study in open literature, direct scattering problem in circular waveguide for partially loaded, lossy and inhomogenous materials is the purpose of this thesis.

The results, obtained in this study serve as the basis for inverse scattering problem for reconstructing the electrical properties of 3-D, arbitrarily shaped, lossy dielectric materials loaded in circular waveguide.

2. DIRECT SCATTERING PROBLEM IN CIRCULAR WAVEGUIDE

2.1 Statement of the Problem

Addressing the forward scattering problem, one considers the spatial domain of object D having conductivity *σ(r)*, dielectric permittivity *ε(r)* and magnetic permeability *μ(r),* embedded in a volume with constant electromagnetic parameters. The sources, generating the electromagnetic field are outside the volume D. If the constitutive parameters of domain D and the incident electric field are known, the total electric field strength can be solved via Fredholm integral equation of the second kind, namely;

$$E^{inc}\left(\vec{r}\right) = E\left(\vec{r}\right) - k_b{}^2 \int\limits_{r' \in D} \overline{\overline{G}}\left(\vec{r}, \vec{r'}\right) v\left(\vec{r'}\right) E\left(\vec{r'}\right) dr' \qquad \textbf{(2.1)}$$

where

$$k_b{}^2(\omega) = \omega^2 \varepsilon_b \mu_b + i\omega\sigma_b, \qquad \textbf{(2.2)}$$

and

$$v(\vec{r}, \omega) = \frac{i\omega\varepsilon(r) - \sigma(r)}{i\omega\varepsilon_b - \sigma_b} - 1 \qquad \textbf{(2.3)}$$

which is called as "object function" or "the electric contrast function". Letting $k(\vec{r}, \omega)$ as the wave number inside the object as a function of position and frequency and $k_b(\omega)$, the wave number outside the object, object function becomes

$$v(\vec{r}, \omega) = \frac{k^2(\vec{r}, \omega)}{k_b^2(\omega)} - 1 \qquad \textbf{(2.4)}$$

Here, the term $\overline{\overline{G}}\left(\vec{r}, \vec{r'}\right)$ is the dyadic Green's function of empty waveguide and explained in detail in Section 2.2. In this study, the volume that the object D is embedded in, is empty circular waveguide. Hence $\sigma_b = 0$ and k_b is equal to k_0, the wave number of free space. Note that, outside the object *D*, $k(\vec{r}) = k_0$ and object equation, given in (2.4), equals to zero.

This solution, determining the scattered field caused by the discontinuity is named as "direct scattering problem". Here, the incident electric field and the constitutive parameters of discontinuity are known.

The main aim of this study is to solve direct scattering problem for object D depicted in Figure 2.1. The time dependency is taken as e^{-jwt} and suppressed. Object D is a lossy dielectric, non-magnetic ($\mu = \mu_0$) and partially loaded in a circular waveguide.

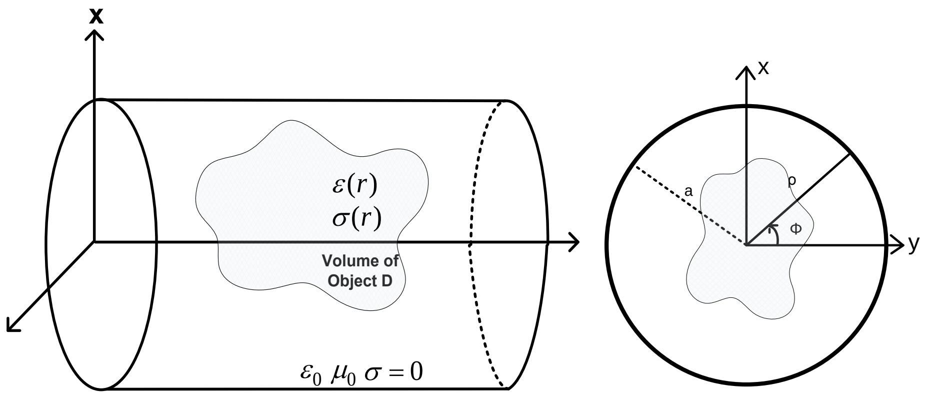

Figure 2.1: An inhomogeneous object located in a circular waveguide (a) longitudinal view (b) cross-section view.

The incident field $\vec{E}^i$ is excited at dominant mode, TE_{11} for circular waveguide where the propagation is along +*z* direction. The electric field, inside the empty waveguide is equal to the incident field. While an object exists inside the waveguide, the total electric field, $\vec{E}^{tot}$, at any given point inside the waveguide is a sum of the incident field $\vec{E}^i$ and the scattered field $\vec{E}^s$, generated by the volume current density inside the object, namely;

$$\vec{E}^{tot} = \vec{E}^i + \vec{E}^s \qquad \textbf{(2.5)}$$

Taking into consideration (2.5) and (2.1), one can easily obtain the expression for the scattered field for the problem depicted in Figure 2.1

$$\overrightarrow{E}^{S} = k_0^{\,2} \int_{r'\in D} \overline{\overline{G}}\left(\vec{r},\vec{r}'\right) v\left(\vec{r}'\right) \overrightarrow{E}\left(\vec{r}'\right) dr' \quad \textbf{(2.6)}$$

In (2.6), $\vec{r} = (\rho, \phi, z)$ and $\vec{r}' = (\rho', \phi', z')$ represents the observation and source points respectively. This equation becomes invalid due to the nature of Green's function where the source and the observation points, r and r' are equal. So as to overcome this problem, an infinitesimally small volume, surrounding the $r = r'$ subdomain, removed from the integral equation and this part of the integral is calculated independently [11]. This removed volume is called as principle volume. This approach leads to alter the (2.6) as below;

$$\overrightarrow{E}^{S} = k_0^{\,2} \lim_{\delta\to 0} \int_{V_D - V_\delta} \overline{\overline{G}}\left(\vec{r},\vec{r}'\right) v\left(\vec{r}'\right) \overrightarrow{E}\left(\vec{r}'\right) dr' - v\left(\vec{r}'\right) \overrightarrow{E}\left(\vec{r}'\right) \overline{L} \quad \textbf{(2.7)}$$

Here, the term $\overline{L}$ is the source dyadic and depends solely on the shape of the removed volume. For some simple volumes, this source dyadic is determined in literature [11,13]. In this study, a pillbox type volume [13] is considered as the removed volume, which can be seen in Figure 2.2.

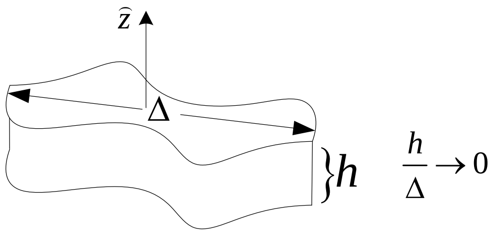

Figure 2.2 : Pill box type principle volume

This type source dyadic equals to $\hat{e}_z \times \hat{e}_z$. Since the current density $J(\vec{r})$ can be expressed in terms of electric field and the dielectric constant of domain due to the volume equivalence theorem [14], as in (2.8)

$$\vec{J}(\vec{r}) = -i\omega[\varepsilon(\vec{r}) - \varepsilon_0]\vec{E}(\vec{r}) \quad \textbf{(2.8)}$$

Substituting source dyadic $\hat{e}_z \times \hat{e}_z$ and volume current density $\vec{J}(\vec{r})$ in (2.8), the field strength, in terms of $\vec{J}(\vec{r})$, can be expressed as below;

$$\overline{E}^{s} = i\omega\mu_0 \lim_{\delta\to 0} \int_{V_D - V_\delta} \overline{\overline{G}}\left(\vec{r},\vec{r}'\right)\vec{J}\left(\vec{r}'\right)dv' + \frac{\vec{J}_z}{i\omega\varepsilon_0} \tag{2.9}$$

The final expression of integral equation for the solution of problem is given with (2.9)

$$-\overline{E}^{i}(\vec{r}) = \frac{\vec{J}(\vec{r})}{i\omega[\varepsilon(\vec{r})-\varepsilon_0]} + i\omega\mu_0 \lim_{\delta\to 0} \int_{V_D - V_\delta} \overline{\overline{G}}\left(\vec{r},\vec{r}'\right)\vec{J}\left(\vec{r}'\right)dv' + \frac{\vec{J}_z}{i\omega\varepsilon_0} \tag{2.10}$$

To determine the unknown term, the volume current density $\vec{J}(\vec{r}')$, in (2.10) is available by the aid of Method of Moments. Details of this numerical method to solve integral equation in (2.10) are covered in Section 2.3.

Thus far, the direct scattering problem is explained and the problem, examining in this study is introduced. Hereafter, dyadic Green's function for circular waveguide is covered in Section 2.2.

2.2 Dyadic Green's Function for Circular Waveguide

Dyadic Green's function for waveguides has firstly been treated by Tai [15]. Readers, interested in derivation of the Dyadic Green's Function for circular waveguide are referred to [15]. In this part, the closed and explicit forms of DGF for circular waveguide are given.

The Dyadic Green's function for circular waveguide is given below;

$$\overline{\overline{G}}\left(\vec{r},\vec{r}'\right) = \frac{i}{4\pi}\sum_{n=0}^{\infty}\sum_{m=1}^{\infty}\begin{bmatrix} \dfrac{2-\delta_0}{\mu^2 I_\mu k_\mu} M_{n\mu}(\pm k_\mu) M_{n'\mu}(\mp k_\mu) \\ +\dfrac{2-\delta_0}{\lambda^2 I_\lambda k_\lambda} N_{n\lambda}(\pm k_\lambda) M_{n'\lambda}(\mp k_\lambda) \end{bmatrix} \quad z \gtrless z' \tag{2.11}$$

where $k_\mu = \sqrt{(k^2-\mu^2)}$, $k_\lambda = \sqrt{(k^2-\lambda^2)}$, $I_\mu = \frac{1}{2}a^2 J_n^2(q_{nm})\left[1-(n/q_{nm})^2\right]$, $\mu = \frac{q_{nm}}{a}$, $\lambda = \frac{p_{nm}}{a}$, $I_\lambda = \frac{1}{2}a^2 J_{n+1}^2(p_{nm})$.

The quantities p_{nm} and q_{nm} are the m^{th} roots of the n^{th} order Bessel function J_n and its derivative J_n' respectively. The kronocker delta $\delta_0 = 1$ for $n=0$ and $\delta_0 = 0$ for

$n \neq 0$. Even and odd components of solenoidal vector wave functions of M and N are not defined specifically, that is $M^{e}_{on\mu}$ is simplified to $M_{n\mu}$ as well as $N_{n\lambda}$, namely;

$$M_{n\mu}\left(\pm k_{\mu}\right)=\nabla\times\left[\hat{z}J_{n}\left(\mu\rho\right)\cos\left(n\phi-\phi_{p}\right)e^{\pm ik_{\mu}z}\right] \qquad \textbf{(2.12)}$$

$$N_{n\lambda}\left(\pm k_{\lambda}\right)=\frac{1}{k}\nabla\times\nabla\times\left[\hat{z}J_{n}\left(\lambda\rho\right)\cos\left(n\phi-\phi_{p}\right)e^{\pm ik_{\lambda}z}\right] \qquad \textbf{(2.13)}$$

In (2.11) and (2.12), the term ϕ_p is 0 for even components and $\pi/2$ for odd components. The general $\overline{\overline{G}}$ is sum of even and odd components. For clarity in print, explicit expression of dyadic green function for empty circular waveguide is given below.

$$\overline{\overline{G}}\left(\vec{r},\vec{r}\,'\right)=\frac{i}{4\pi k_0^2}\sum_{n=0}^{\infty}\sum_{m=1}^{\infty}\left(2-\delta_0\right).\left\{\begin{array}{l}\hat{\rho}\hat{\rho}'\left[n^2k_1M_{\rho}M_{\rho'}e_{1\mu}+k_2N_{\rho}N_{\rho'}e_{1\lambda}\right]\\+\hat{\rho}\hat{\phi}'\left[nk_1M_{\rho}M_{\phi'}e_{1\mu}-nk_2N_{\rho}N_{\phi'}e_{1\lambda}\right]\\+\hat{\rho}\hat{z}\left[k_3N_{\rho}N_{z'}\left(\pm e_{1\lambda}\right)\right]\\+\hat{\phi}\hat{\rho}'\left[nk_1M_{\phi}M_{\rho'}e_{1\mu}-nk_2N_{\phi}N_{\rho'}e_{1\lambda}\right]\\+\hat{\phi}\hat{\phi}'\left[k_1M_{\phi}M_{\phi'}e_{1\mu}+n^2k_2N_{\phi}N_{\phi'}e_{1\lambda}\right]\\+\hat{\phi}\hat{z}\left[nk_3N_{\phi}N_{z'}\left(\mp e_{1\lambda}\right)\right]\\+\hat{z}\hat{\rho}'\left[k_3N_{z}N_{\rho'}\left(\mp e_{1\lambda}\right)\right]\\+\hat{z}\hat{\phi}'\left[nk_3N_{z}N_{\phi'}\left(\pm e_{1\lambda}\right)\right]\\+\hat{z}\hat{z}\left[k_4N_{z}N_{z'}e_{1\lambda}\right]\end{array}\right\}, \qquad \textbf{(2.14)}$$

The expansions of terms in (2.14) are juxtaposed below.

$$N_z=J_n\left(\lambda\rho\right)\cos\left(n\phi-\phi_p\right) \qquad M_{\phi}=J'_n\left(\mu\rho\right)\cos\left(n\phi-\phi_p\right) \qquad N_{\rho}=J'_n\left(\lambda\rho\right)\cos\left(n\phi-\phi_p\right)$$

$$M_{\rho}=\frac{1}{\rho}J_n\left(\mu\rho\right)\sin\left(n\phi-\phi_p\right) \qquad N_{\phi}=\frac{1}{\rho}J_n\left(\lambda\rho\right)\sin\left(n\phi-\phi_p\right) \qquad e_{1\lambda}=e^{ik_{\lambda}|z-z'|},\ e_{1\mu}=e^{ik_{\mu}|z-z'|}$$

$$k_1=\frac{k^2}{\mu^2I_{\mu}k_{\mu}} \qquad k_2=\frac{k_{\lambda}}{\lambda^2I_{\lambda}} \qquad k_3=\frac{i}{I_{\lambda}} \qquad k_1=\frac{\lambda^2}{I_{\lambda}k_{\lambda}}$$

2.3 Solution by the Method of Moments

More developments in scattering theory have resulted in research of complicated problems that are not being able to be solved through analytical solutions. Numerical methods and use of computers are a primitive approach for the solution of such problems. In this study, the Method of Moments is utilized.

Solving the integral equations, such as (2.10), by the aid of computers, one may use numerical techniques by converting this integral equation into a linear system. To this aim, the integral equations are converted to matrix form by means of basis functions and weighting functions. Evaluating the elements in matrix form, the desired parameters are obtained.

A similar problem, a dielectric material loaded inside a rectangular waveguide formulation of direct scattering problem, is handled by J.J.H. Wang [9]. In this approach, the object volume is divided into L cells and the electric field, also the current density is assumed to be uniform in each cell. In this study, two types of cell division is proposed and detailed in Section 2.5. The current density can be expressed as below

$$J(r)=\sum_{k}^{3}\sum_{l=1}^{L}J_l^k \mathrm{B}_l^k(r) \tag{2.15}$$

Here, $k=1,2,3$ denotes (x,y,z) for cartesian and (ρ,ϕ,z) for cylindrical coordinate systems respectively. The subscript “l“ represents the l^{th} cell. B_l^k is basis function, defined as

$$\mathrm{B}_l^k(r)=u_k \mathrm{P}_l(r) \tag{2.16}$$

where u_k is unit vector and

$$\mathrm{P}_n(r)=\begin{cases}1, & r\in\Delta D_n\\ 0, & otherwise\end{cases} \tag{2.17}$$

The weighting function is defined as

$$W_q^p(r)=\delta(r-r_q)\widehat{u}_p \tag{2.18}$$

Determining the basis and weighting functions, the equivalent current density is replaced into the main integral equation (2.9). The scalar product defined as

$$\langle f, g \rangle = \int_V f.g\, dv \tag{2.19}$$

is performed, using the weighting function. $W_q^p(r)$. Here "*p*" represents the axis $(x, y, z$ or ρ, ϕ, z etc.$)$ and "*q*" the number of cell. The following set of equations pursues this moment generating procedure as below;

$$\sum_{k=1}^{3}\sum_{l=1}^{L} J_l^k \mathrm{A}_{kl}^{pq} = C^{pq} \tag{2.20}$$

$$C^{pq} = -E^i(r_q) \tag{2.21}$$

In Section 2.4, the matrix equations and the evaluations of terms in matrix forms are covered.

2.4 Matrix Equations

The inner product between $\vec{J}(\vec{r}\,')$ and $\overline{\overline{G}}(\vec{r},\vec{r}\,')$ may be represented as;

$$\overline{\overline{G}}(\vec{r},\vec{r}\,').\vec{J}(\vec{r}\,') = \begin{bmatrix} G_{\rho\rho'}(\vec{r},\vec{r}\,') & G_{\rho\phi'}(\vec{r},\vec{r}\,') & G_{\rho z'}(\vec{r},\vec{r}\,') \\ G_{\phi\rho'}(\vec{r},\vec{r}\,') & G_{\phi\phi'}(\vec{r},\vec{r}\,') & G_{\phi z'}(\vec{r},\vec{r}\,') \\ G_{z\rho'}(\vec{r},\vec{r}\,') & G_{z\phi'}(\vec{r},\vec{r}\,') & G_{zz'}(\vec{r},\vec{r}\,') \end{bmatrix} \begin{bmatrix} J_{\rho'}(\vec{r}\,') \\ J_{\phi'}(\vec{r}\,') \\ J_{z'}(\vec{r}\,') \end{bmatrix} \tag{2.22}$$

where r is observation point and r' is the source point with components *(ρ,ϕ,z)* and *(ρ',ϕ',z')* respectively.

Considering the integral equation (2.10) and moment generating procedure, the term A_{kl}^{pq} in (2.20) can be discretized as below;

$$A_{kl}^{pq} = i\omega\mu_0 Q_{lq}^{pk} + \frac{\delta_q^l}{i\omega}\left[\frac{\delta_k^p}{\varepsilon(r_q)-\varepsilon_0} + \frac{\delta_3^k \delta_3^p}{\varepsilon_0}\right] \tag{2.23}$$

Here the δ_k^p is the "kronecker delta", takes the value 1 when $p = q$ and 0 otherwise, that is identity element for off-diagonal and out of volume *D*, and

$$Q_{lq}^{pk} = \int\limits_{\Delta V_l} G^{pk}(r_q, r')dV' \qquad \textbf{(2.24)}$$

Now the matrix equation can be derived by letting $\left[G_{x_p x_q}\right]$ an $N \times N$ matrix, where N is the number of cells. The elements of this matrix are A_{kl}^{pq}, defined by (2.23). Also let N dimensional vectors $\left[J_{x_p}\right]$ and $\left[E_{x_p}^{i}\right]$ be

$$\left[J_{x_p}\right] = \begin{bmatrix} J_{x_p}(r_1) \\ . \\ . \\ . \\ J_{x_p}(r_N) \end{bmatrix}, \qquad \left[E_{x_p}^{i}\right] = \begin{bmatrix} E_{x_p}^{i}(r_1) \\ . \\ . \\ . \\ E_{x_p}^{i}(r_N) \end{bmatrix} \qquad \textbf{(2.25)}$$

Substituting (2.20) with preceding formulas, one obtains the matrix equation as

$$\begin{bmatrix} \left[A_{\rho\rho'}\right] \left[A_{\rho\phi'}\right] \left[A_{\rho z'}\right] \\ \left[A_{\phi\rho'}\right] \left[A_{\phi\phi'}\right] \left[A_{\phi z'}\right] \\ \left[A_{z\rho'}\right] \left[A_{z\phi'}\right] \left[A_{zz'}\right] \end{bmatrix}_{3N \times 3N} \begin{bmatrix} \left[J_{\rho}\right] \\ \left[J_{\phi}\right] \\ \left[J_{z}\right] \end{bmatrix}_{1 \times 3N} = -\begin{bmatrix} \left[E_{\rho}^{i}\right] \\ \left[E_{\phi}^{i}\right] \\ \left[E_{z}^{i}\right] \end{bmatrix}_{1 \times 3N} \qquad \textbf{(2.26)}$$

or in short, $[A][J] = -\left[E^{i}\right]$. Here the matrix elements $A_{x_p x_q}$ are the ones defined by (2.23). Knowing the incident field and performing the dyadic Green's function integrals, one can obtain the volume current density by inverting the left side of (2.26), matrix $A_{x_p x_q}$ and multiply by matrix $E_{x_p}^{i}$, namely;

$$[J] = -[A]^{-1}\left[E^{i}\right] \qquad \textbf{(2.27)}$$

In order to obtain the electric field at any point r_v, generated by the current density, which is found by (2.27), can be derived by multiplying the current matrix $[J]$ with matrix $[A]$ just letting the observation point as r_v.

2.5 Determination of Cell Type

In this study, the shapes of cells, namely ΔV_n, are performed both in cartesian and cylindrical coordinates. Hence, the evaluation of (2.24) depends on the cell type and the elements vary in two cell-division approaches. The volume variable of integration is defined in two coordinate systems as

$$\Delta V_n^{'} = \begin{cases} \Delta x'.\Delta y'.\Delta z', & \text{in cartesian coordinates} \\ \rho'.\Delta\rho'.\Delta\phi'.\Delta z', & \text{in cylindirical coordinates} \end{cases} \quad \textbf{(2.28)}$$

As seen in (2.28), the volume variable of integration differs in both coordinate systems. Due to (2.28), one should consider the difference in the evaluation of the integrals of $M'^{e}_{on\mu}$ and $N'^{e}_{on\lambda}$ vector wave functions.

As mentioned before, two types of cells are performed in the solution of direct scattering problem in circular waveguide. In this section, these two types of cells are introduced and equations for each one given in sub-sections.

2.5.1 Rectangular Cell Type Division in Cartesian Coordinates

First attempt to solve the problem, explained in Section 2.1, is performed with rectangular type cell. The illustration of this type of cell is given with Figure 2.3.

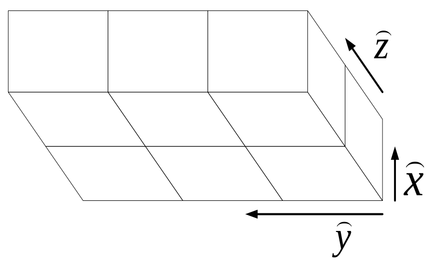

Figure 2.3 : Illustration of rectangular type cell

If the observation and source points are different one from the other, then the terms, given in (2.13), converges with direct summation due to the term $ik_{\mu,\lambda}\left|z_q - z_p\right|$. However, if the observation and source points are equal, the matrix elements converge very slowly. A solution is proposed for rectangular waveguide by J J Wang [9] using partial summation technique. Some slowly convergent infinite series can be analytically expressed. For instance, $\sum_{m=1}^{\infty}\frac{\sin(mx)}{m} = \frac{\pi - x}{2}$ and can be applied to kind some terms for integrals of DGF of rectangular waveguide. Also, there are other of analytic expressions for infinite series in expansion of Green's functions' integral for rectangular waveguide [9].

As far as we could see, no appropriate terms exist in the terms of DGF for circular waveguide to apply partial summation for this type division. In Figure 2.4, a comparison is given between Mode Matching Method [8] and rectangular cell division. Dominant mode TE_{11} is excited and $|S_{11}|$ is chosen for comparison. Tho object of width 5 cm is fully loaded inside the waveguide. Relative permittivity, ε_r of the object is 4. Observation point is selected approximately $\lambda/2$ away the object. Mode Matching Method is an analytic method, utilizing from boundary conditions and chosen as a reference solution for fully loaded waveguide problems. As can be seen in Figure 2.4, the solution with rectangular cell type becomes invalid for increasing modes of Green's function.

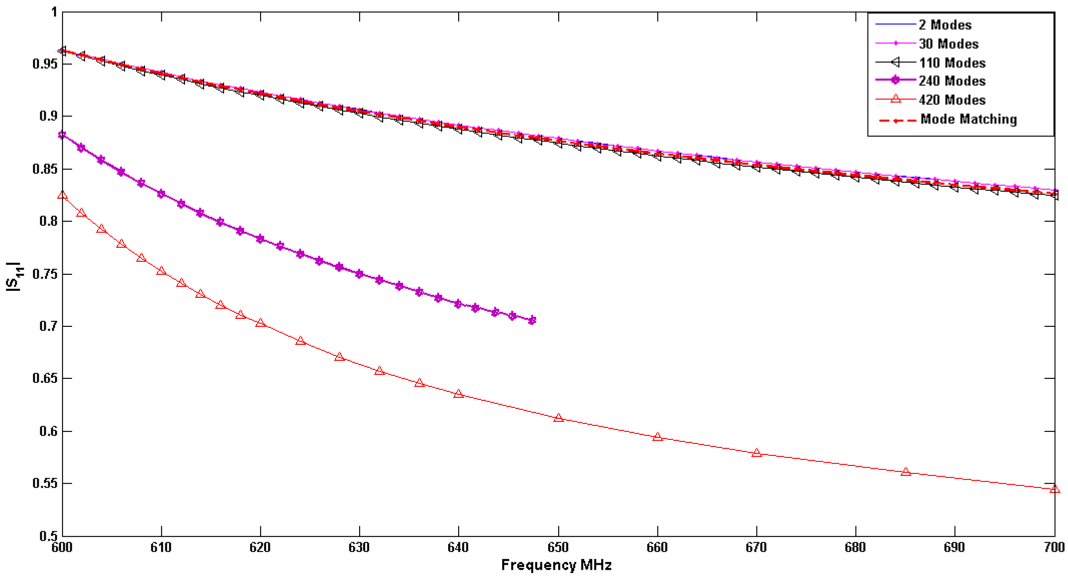

Figure 2.4 : Comparison between MMM and RCTD for higher modes

Rectangular cell division is quite satisfactory up to first 110 modes. Nevertheless, to evaluate the DGF properly, the convergence should be satisfied. If one would know the excited modes caused by the object, this cell division would be adequate, but it's not enough for a complete solution.

2.5.1.1 Discretization for MoM in case of rectangular cell type divison

Due to the dependency of the components of dyadic Green's function for circular waveguide on *(ρ',ϕ',z')*, if one selects the *x,y,z* coordinates, the variables of integration *dx* and *dy* become constant. Hence, only the terms, involving *z'* components exist as integrands. As seen in (2.14), only the exponential terms are performed in integral expression. Hence, "$\Delta x \times \Delta y$" and any other term in (2.14) become constant (Δx and Δy are the length of cubic cell in given direction). Shortly, (2.24) becomes

$$Q_{lq}^{pk} = \Delta x \times \Delta y \times \frac{i}{4\pi k_0^2} \sum_{n=0}^{\infty} \sum_{m=1}^{\infty} F_{mn}^{pk} I \qquad \textbf{(2.29)}$$

where

$$F_{mn}^{pk} = \text{[the (m,n)}^{th} \text{ term of } G^{pk} \text{ that non-involving } z' \text{ component]} \qquad \textbf{(2.30)}$$

and

$$I = \begin{cases} \dfrac{2}{ik_{\mu,\lambda}}\left(e^{ik_{\mu,\lambda}\Delta z/2} - 1\right)e^{ik_{\mu,\lambda}\left|z_q - z_p\right|}, & \text{if} \quad z_q = z_p \\ \dfrac{2}{k_{\mu,\lambda}}\sin\left(k_{\mu,\lambda}\dfrac{\Delta z}{2}\right)e^{ik_{\mu,\lambda}\left|z_q - z_p\right|}, & \text{otherwise} \end{cases} \qquad \textbf{(2.31)}$$

where z_q and z_p are the observation and source points, respectively.

In Section 2.5.2, the proposed cell tpye instead of rectangular cell and its evaluation for discretization in (2.20) is handled.

2.5.2 Pie Cell Type Division in Cylindrical Coordinates

For a full analysis of direct scattering problem in circular waveguide, since the rectangular cell type becomes invalid, another approach is proposed with pie cell type. The illustration of this type cell is given with Figure 2.5.

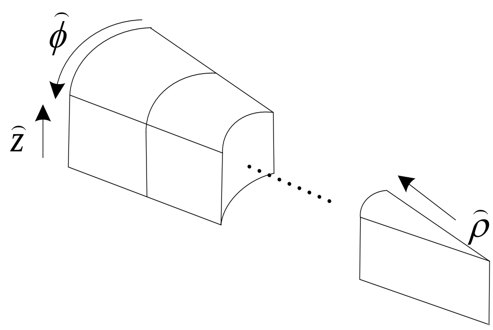

Figure 2.5 : Illustration of pie cell type

The distribution of the cells along the cross-section of the waveguide is given with Figure 2.6. In Figure 2.6, note that the number of cells, surrounding the center of the cross-section are two. The importance of number of cells, surrounding the center is construed afterward. The chords of all cells are desired to be equal and for to do that, an adaptive mesh is implemented. Each ring has cells, two times of its location, and increments in ρ direction are equal. For instance, at the 5th ring, there are 10 cells.

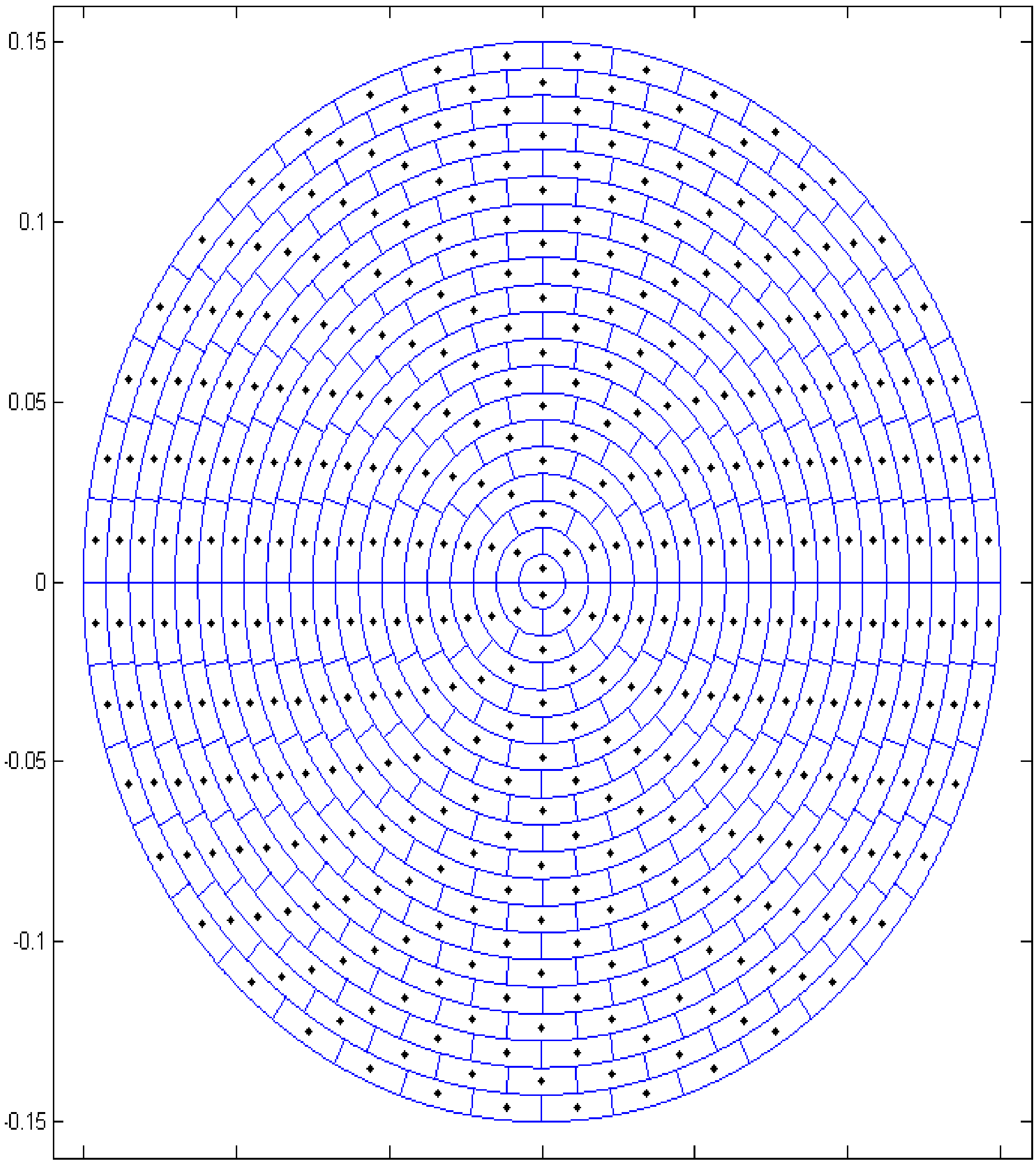

Figure 2.6: Distribution of pie cells along the cross section of waveguide

Many trials have been done to optimize the efficiency of pie cell division. Below, a summary of optimization for pie cell division is given. From Figure 2.7 to 2.10, results are given for fully loaded dielectric with relative permittivity $\varepsilon_r = 4$. The cell distribution is set up as two cells surrounding the center of cross- section as in Figure 2.6.

First, the number of modes in the calculation of (2.23) summation is restricted to 3 and the effect of cell number is tested. In Figure 2.7 $|S_{11}|$ variations with respect to frequency are plotted for different number of cells and compared with the result obtained via Mode Matching Method.

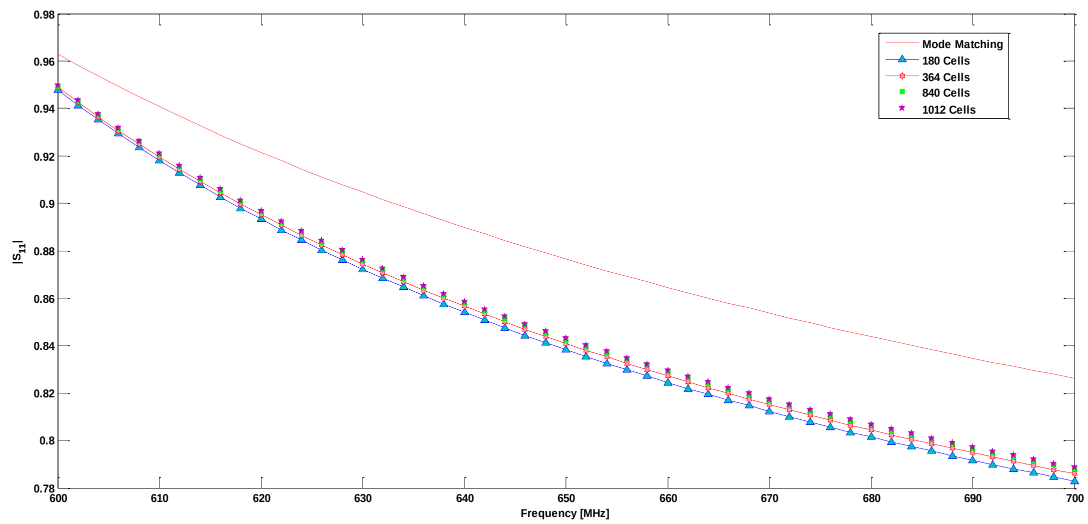

Figure 2.7: Effect of cell number on accuracy of pie cell divison for 3 modes summation

As can be seen in Figure 2.7, there is no much difference between 860 cells and 1012 cells. Hence, to improve the accuracy, increasing the cell number for fewer modes is not an efficient way. The error between the analytic solution and MoM result for 1012 cells, is approximately 1.37% and 4.5%., for minimum frequency and maximum frequency, respectievly.

Increasing the number of modes in calculation of (2.24), up to 30, improves the results as shown in Figure 2.8. At minimum frequency, for 1012 cells, error is approximately 1.1% and that is equal to of 760 cells. Also, the error for 144 cells with 30 modes summation is close to of 1012 cells with 3 modes summation.

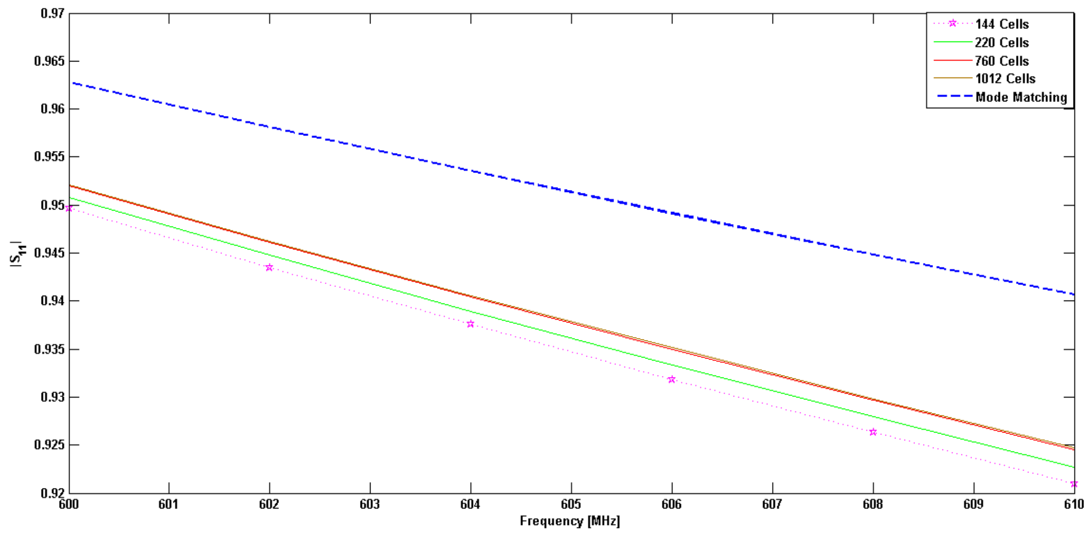

Figure 2.8: Effect of cell number on accuracy of pie cell divison for 30 modes summation

In Figure 2.9, a comparison is given for 760 cells division between 110 modes and 30 modes. Increasing the modes in calculation of DGF, had not been a remedy and error remains stable.

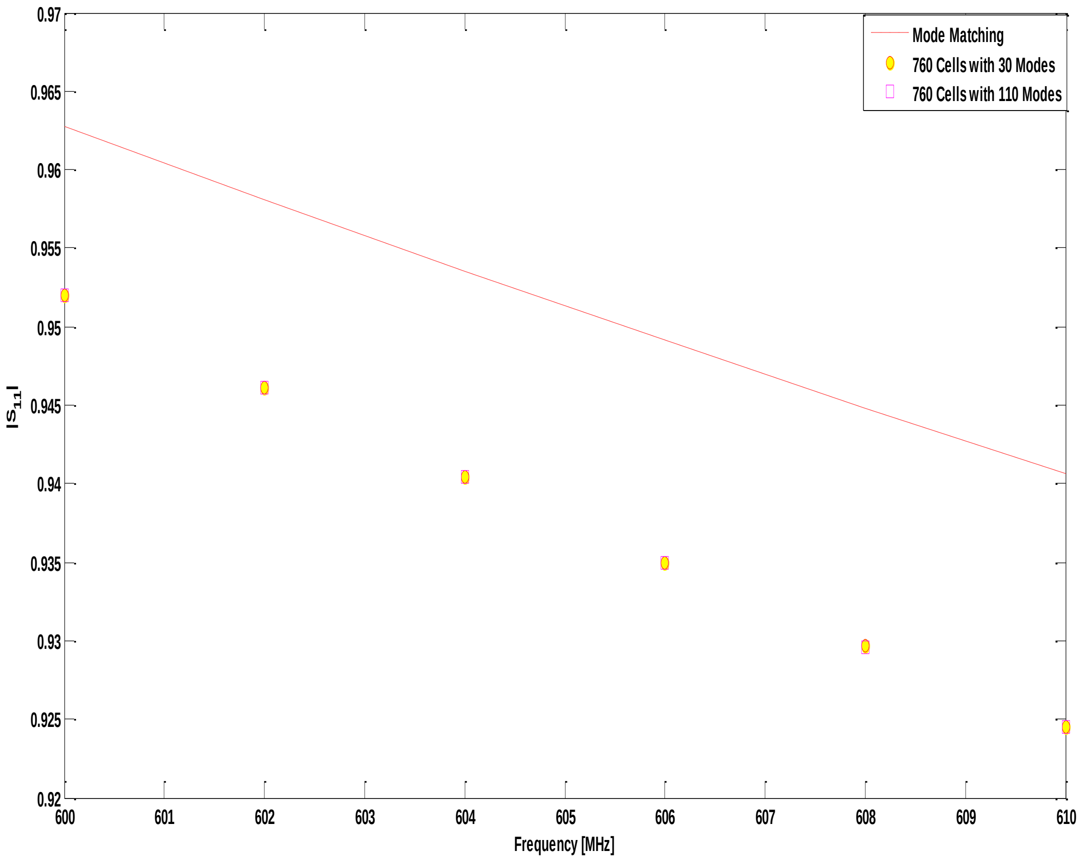

Figure 2.9: Effect of higher number of modes on accuracy of pie cell divison

Another attempt to optimize the results is to increment the number of cells surrounding the center point of cross-section. As implemented and explained in Figure 2.6, adaptive mesh structure is used again, that is, if the cell number, surrounding the center is X, than the number of cells in the following rings are 2X, 4X, 6X and so on.

In Figure 2.10, a comparison between two division is given. It's interesting that although decreasing the total number of cells, an increment in number of cells, surrounding the center, resulted in a recovery. For instance, The number of cells, surrounding the origin are increased from 2 to 7 and the total number of cells are decreased from 760 to 396. This approach decreased the error from 1.1% to 1.08%. So, one obtains less computation load and error.

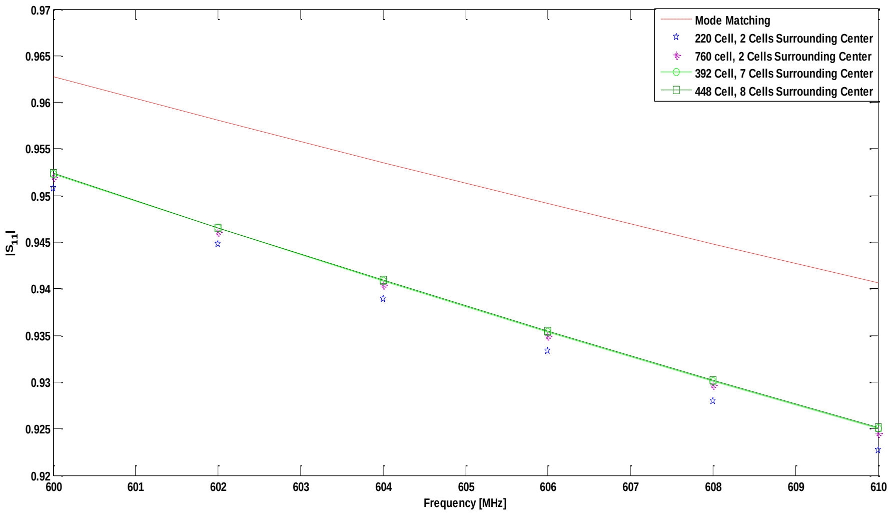

Figure 2.10: Effect of increment in cell number surrounding center of cross-section

For optimizing the numerical calculations, another attempt is decreasing the cell dimensions. Since the computational load increases drastically with number of cells, a setup is prepared instead of the one proposed above. Setup is a three-layered model, with relative permittivities 6,8 and 4. Each layer is equal and 1 cm width in *z*-direction, which is approximately λ/50. The cell dimensions in ρ and ϕ directions are equal and approximately around λ/45. The number of cells, around the origin is 7. The result for this setup is given in Figure 2.11. Decreasing the cell dimension in *z*-direction gives a remedy. The error between the results obtained via MMM and MoM for the lowest frequency of this setup is 0.16%.

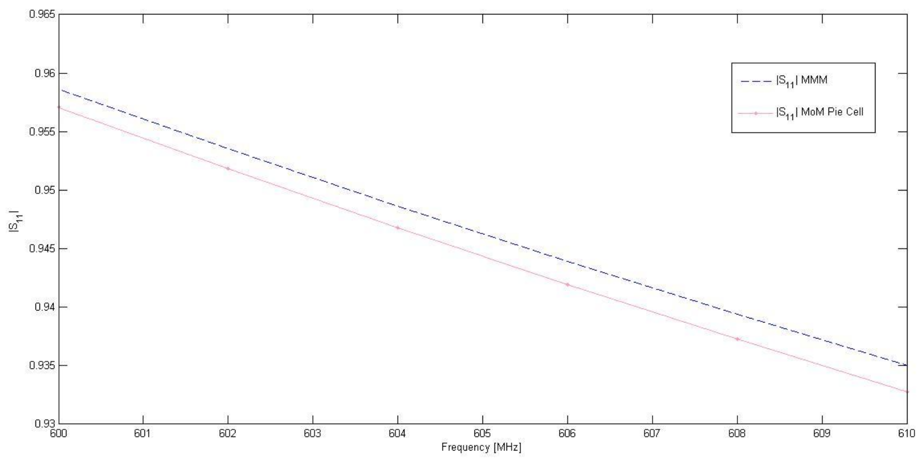

Figure 2. 11: Effect of decreasing cell dimension in z-direction

Up to here, a summary is given for optimization of pie cell type division. It has been shown that, an increment in the number of cells, surrounding the center results in a better accuracy. The interesting result is, this remedy is valid for less number of total cells. Namely, incrementing of cells around the center decreases the computation load and improves accuracy. If the cell dimension in ρ and ϕ directions are close, it gives a better accuracy.

As mentioned before, direct summation causes divergence for rectangular cell type division. In Figure 2.12, the value of the maximum term of diagonal elements for A_{kl}^{pq} is shown with respect to number of modes. For rectangular cell type division, a divergence occurs, hence pie type cell division is proposed. In the same figure, convergence for pie type cell division can be seen.

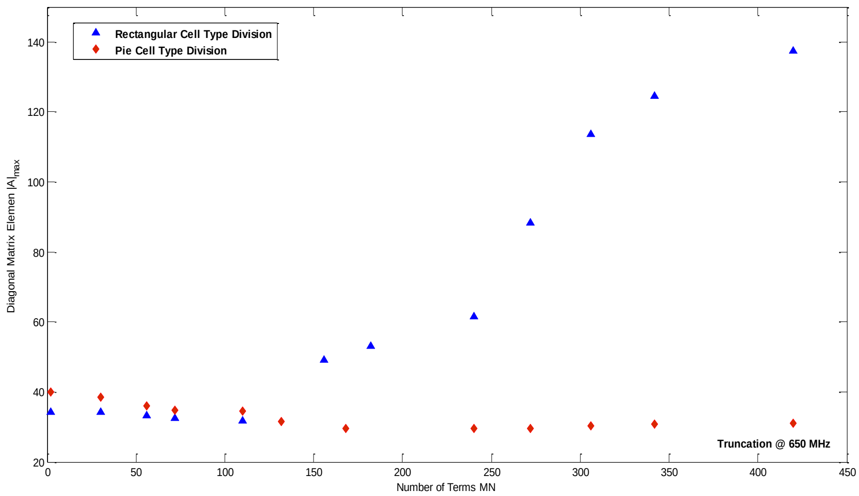

Figure 2.12 : Convergence of direct summation with truncation for rectangular cell and pie cell type division

2.5.2.1 Discretization for MoM in case of pie cell type divison

If one works in cylindrical coordinates, contrary to cartesian coordinates, all integrands in (2.14) should be integrated. The detailed integral expressions, involving ρ' components, are given in Appendix A, B and C for several types of integrals of components in (2.15). The integral of components, involving z' terms are same as in (2.31). For terms, such as $\cos(n\phi')$, the integral is simply of the sinusoidal functions. Any other term, not involving ρ', ϕ' and z' terms, becomes constant.

$$Q^{pk} = \frac{i}{4\pi k_0^2} \sum_{n=0}^{\infty} \sum_{m=1}^{\infty} F_{mn}^{pk} IG^{pk} \tag{2.32}$$

where

F_{mn}^{pk} = [the (m,n)th term of G^{pk} that non-involving ρ', ϕ', z' component] **(2.33)**

$$I = \begin{cases} \dfrac{2}{ik_{\mu,\lambda}}\left(e^{ik_{\mu,\lambda}\Delta z/2} - 1\right)e^{ik_{\mu,\lambda}\left|z_q - z_p\right|}, & \text{if} \quad z_q = z_p \\ \dfrac{2}{k_{\mu,\lambda}}\sin\left(k_{\mu,\lambda}\dfrac{\Delta z}{2}\right)e^{ik_{\mu,\lambda}\left|z_q - z_p\right|}, & \text{otherwise} \end{cases} \tag{2.34}$$

G^{pk} takes values depending on *(p,k)* indices and excitation mode. For *(p,k)* being (1,1), (2,1) for TE modes and (p,2) for TM modes;

$$G^{pk} = \left\{ \int_{\rho'-\frac{\Delta\rho}{2}}^{\rho'+\frac{\Delta\rho}{2}} J_n(\beta\rho')d\rho' \times \frac{-(\cos(n(\phi+\frac{\Delta\phi}{2})-\phi_p)-\cos(n(\phi-\frac{\Delta\phi}{2})-\phi_p))}{n} \right\} \tag{2.35}$$

Besides, for *(p,k)* being (p,1) for TM modes and (1,2), (2,2) for TE modes;

$$G^{pk} = \left\{ \int_{\rho'-\frac{\Delta\rho}{2}}^{\rho'+\frac{\Delta\rho}{2}} J'_n(\beta\rho')d\rho' \times \frac{(\sin(n(\phi+\frac{\Delta\phi}{2})-\phi_p)-\sin(n(\phi-\frac{\Delta\phi}{2})-\phi_p))}{n} \right\} \tag{2.36}$$

and when *(p,k)* is (p,3), the term G^{pk} has no value for TE modes but for TM modes

$$G^{pk} = \left\{ \int_{\rho'-\frac{\Delta\rho}{2}}^{\rho'+\frac{\Delta\rho}{2}} \rho' J'_n(\lambda\rho')d\rho' \times \frac{(\sin(n(\phi+\frac{\Delta\phi}{2})-\phi_p)-\sin(n(\phi-\frac{\Delta\phi}{2})-\phi_p))}{n} \right\} \tag{2.37}$$

where β equals to μ for TE modes and λ for TM modes and ϕ_p is *0* for even components and $\pi/2$ for odd components. Here, *M* vector wave functions describe TE modes, while *N* vector wave functions describe TM modes.

3. NUMERICAL RESULTS

In this section, numerical results are given for the solution of direct scattering problem in circular waveguide. Approaches for results are Method of Moment, Mode Matching Method and commercial software HFSS.

Mode Matching method is used as a reference for comparison of fully loaded objects. Cross-section filled objects' constitutive parameters are at most a function of *z*. The commercial software HFSS requires the waveguide to be ended with perfectly matched layer to measure S_{11} properly. This results in impossibility of S_{21} measurement. Hence, the phase of S_{21} can not be measured by HFSS. For lossless materials, $\sum_{i,j} |S_{ij}|^2 = 1$. Using this property, modules of S_{21} values for lossless materials are calculated for HFSS results via

$$\left|S_{21}\right| = \left(1 - \left|S_{11}\right|^2\right)^{\frac{1}{2}} \tag{3.1}$$

As shown in Section 2.5.1, rectangular cell type in MoM can be satisfactory if the number of modes generated by the discountinity is less than approximately first 100 modes. For Rectangular Cell Type Division (RCTD), up to 30 modes in evaluation of DGF is used in this section.

The results show the consistency of proposed methods. Modules and phases of S_{11} and S_{21}, which carry the information about reflected and transmitted fields at the input and output ports of waveguide, are chosen for comparison. The first and the second cut-off frequencies of circular waveguide for the geometry depicted in Figure 2.1 are 586 MHz and 765 MHz, respectively. To operate in the dominant mode region, the freqency interval of 600 MHz – 700 MHz is chosen.

The first example consists of a three-layered object, which fills the cross-section of waveguide. The obstacle has constant relative permittivities ε_{r1}=6 , ε_{r2}=8, ε_{r3}=4 in each layer, that has same length in z direction which is 1 cm. Comparison of S parameters is done between three different and independent approaches which are Method of Moments , Mode Matching Method and HFSS. Amplitude and phase of

S_{11} and S_{21} parameters that are obtained by these methods are shown in Figure 3.1 and Figure 3.2 respectively.

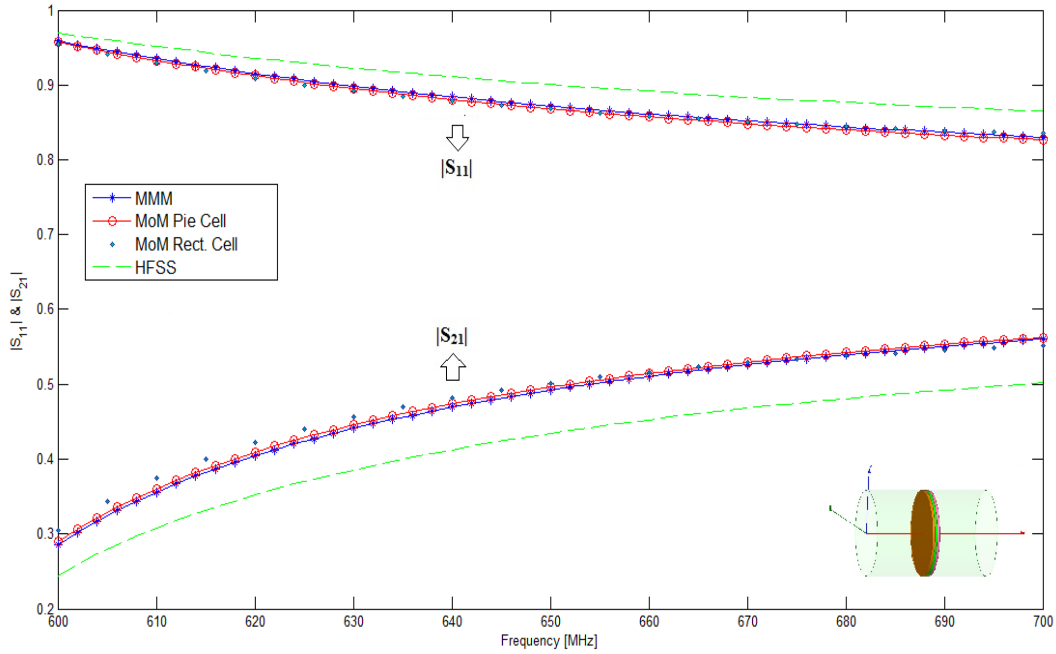

Figure 3.1 : Comparison of $|S_{11}|$ & $|S_{21}|$ for cross-sectional filled with lossless material

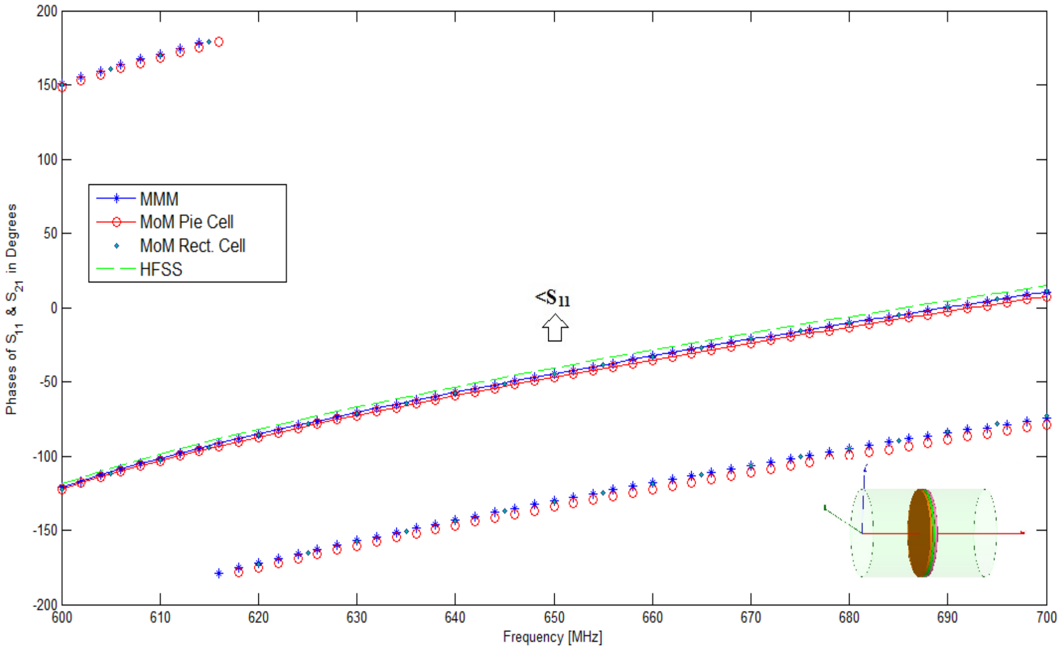

Figure 3.2 : Comparison of $<S_{11}$ & $<S_{21}$ for cross-sectional filled with lossless material

Since the dominant mode excited, the discountinity inside the waveguide only generates the dominant mode. RCTD gives satisfactory results up to approximately first 110 modes. Hence the results obtained by MoM for RCTD is very close to that of MMM. For fully loaded and lossless object, as to MMM, the error for PCTD and RCTD is around 0.16% at lowest frequency for $|S_{11}|$. This sort oIt is also shown that PCTD gives better accuracy as to RCTD. The results, obtained by HFSS, gives error around 4%. The consistency between MMM and MoM for both RCTP and PCTP is shown.

The three-layered object, mentioned above, is treated as a lossy structure in addition. Each layer has a complex part, $\varepsilon^{"} = \sigma / \omega\varepsilon_0$. To obtain a loss tangent around 0.001, the conductivities of lossy materials are chosen as $\sigma_1 = 2{,}55\text{x}10^{-4}$ *(S/m)* $\sigma_2 = 3{,}55\text{x}10^{-4}$ *(S/m)*, $\sigma_3 = 1{,}55\text{x}10^{-4}$ *(S/m)*, respectively. Amplitude of S_{11} and S_{21} parameters for three-layered, lossy model are shown in Figure 3.3.

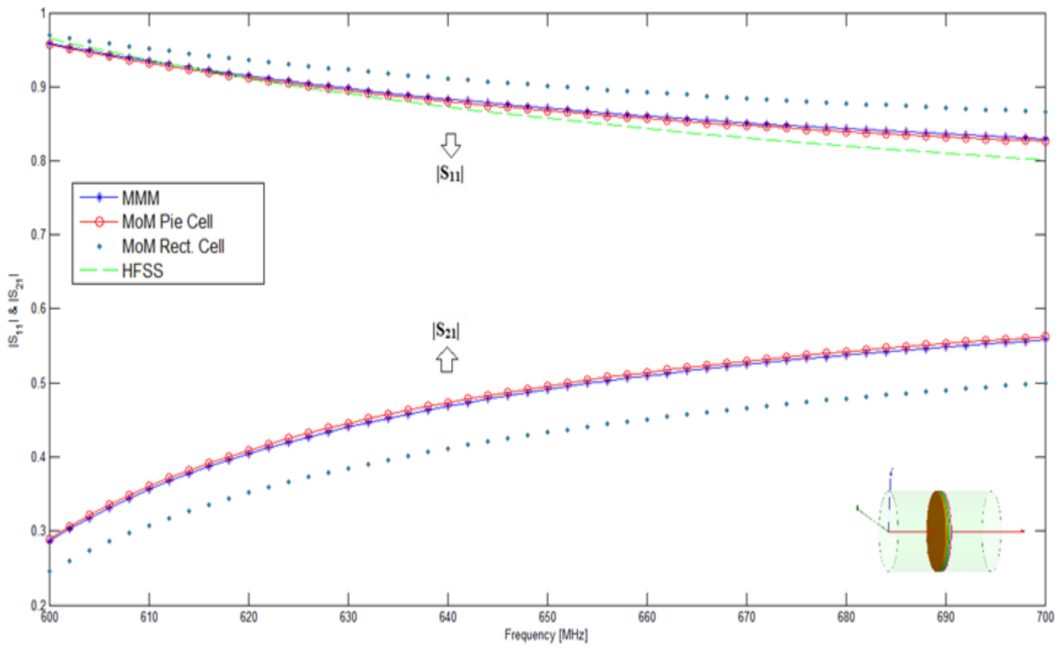

Figure 3.3 : Comparison of $|S_{11}|$ & $|S_{21}|$ for cross-sectional filled with lossy material

Also, phase of S_{11} and S_{21} parameters for three-layered, lossy model are shown in Figure 3.4. Phase results for MoM follows MMM with a little amount of shift. Since a lossy object is determined, only phase of S_{11} could be obtained via HFSS. Phase of S_{11} for HFSS, follows the trace of other methods.

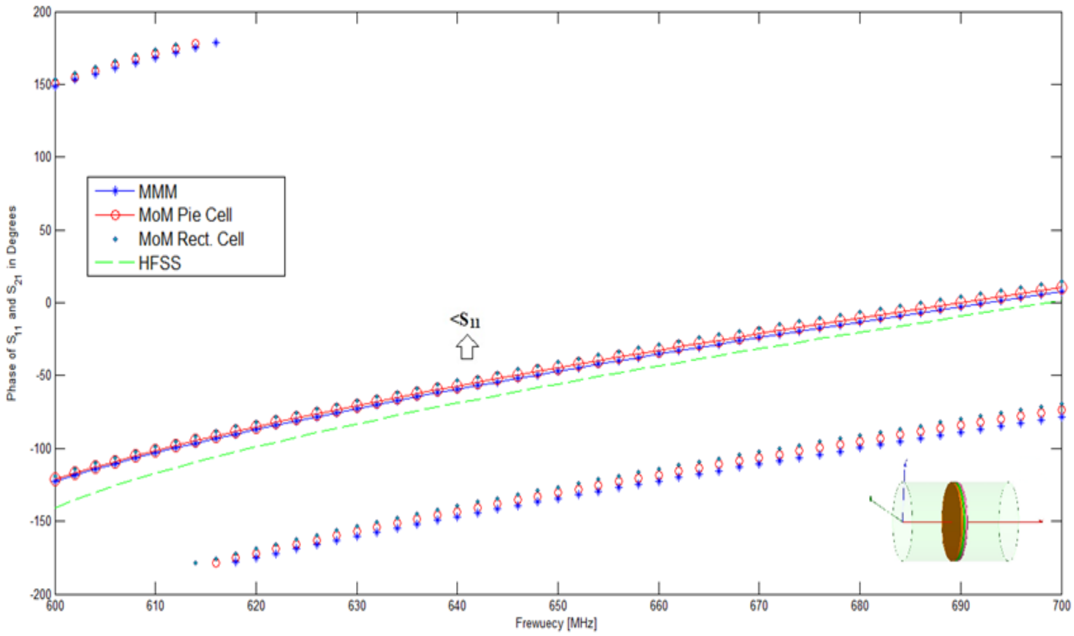

Figure 3.4 : Comparison of <S_{11} & <S_{21} for cross-sectional filled with lossy material

Adding a loss tangent around 0.001 for fully loaded object, alters the consistency of the proposed methods. MoM for PCTD gives an error around 0.2% at lowest frequency for $|S_{11}|$. Loss adittion results in higher modes to be produced. In this case MoM for RCTD becomes insufficient. Because, analyzing the higher modes requires to truncate the sum of integrals of DGF at a higher level. That causes the results of MoM for RCTD to diverge as shown in Figure 2.12. The influence of conductivity on RCTD is that error increases to around 1.1%. HFSS gives worsening results for this setup.

To see the consistency of the proposed methods for high lossy dielectrics, a high lossy setup is simulated. The object is composed of three layers with complex permittivities 6+4i, 8+9i and 4+3i respectively (The complex parts are calculated at 600 MHz frequency). The results for high lossy dielectric object is given for amplitude of S parameters in Figure 3.5. In addition, in Figure 3.6, phase of S parameters are given.

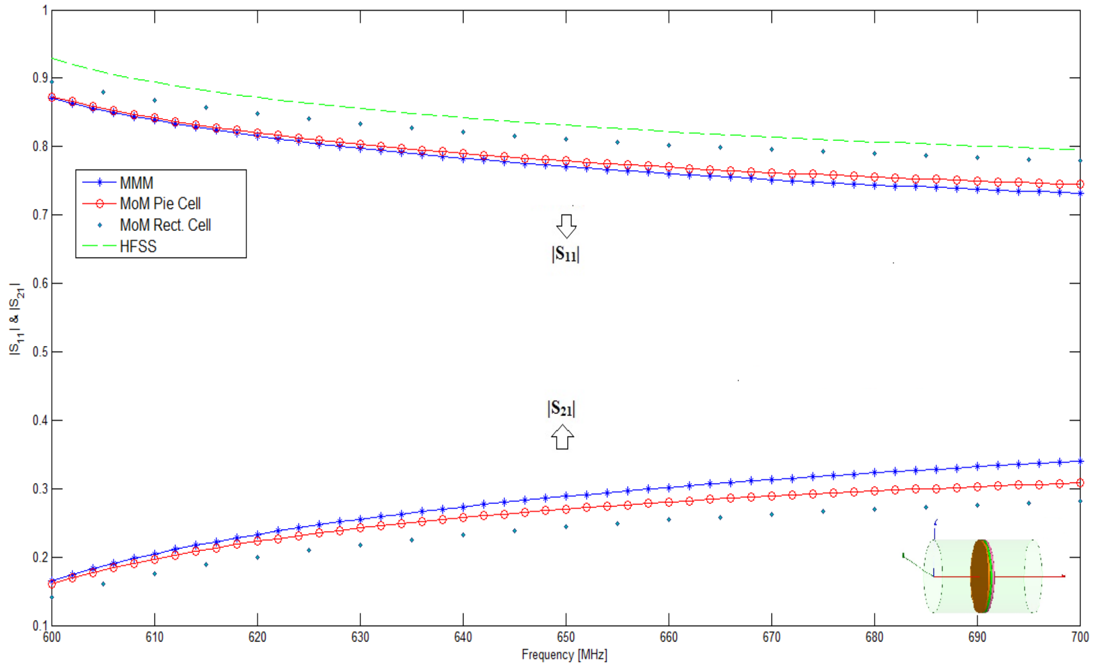

Figure 3.5 : Comparison of $|S_{11}|$ & $|S_{21}|$ for cross-sectional filled with high lossy material

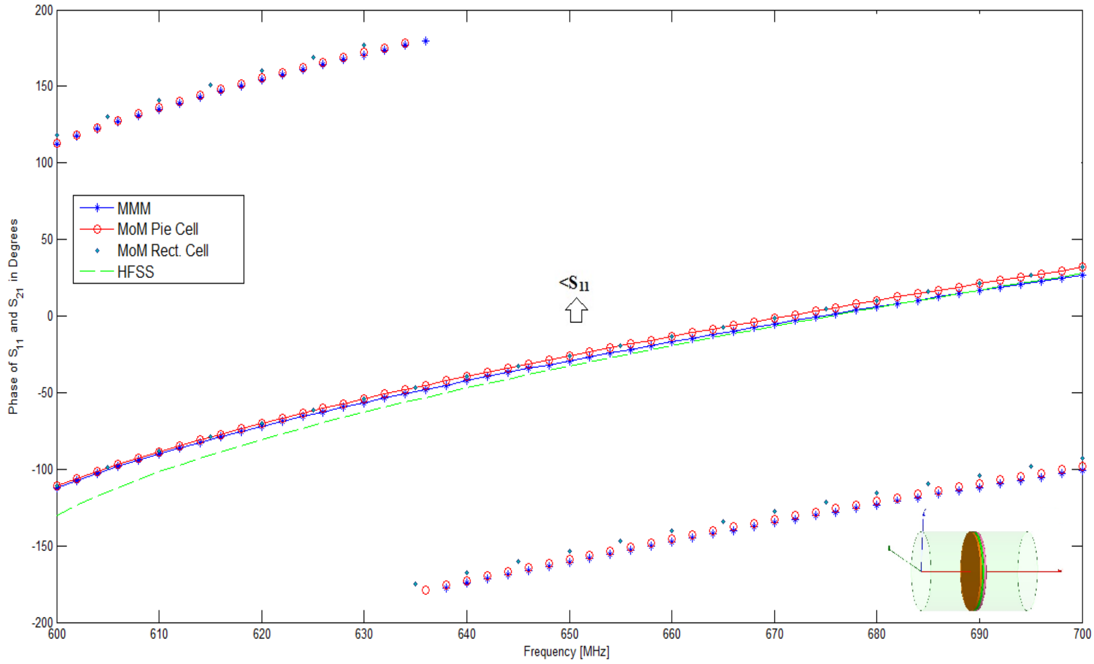

Figure 3.6 : Comparison of $<S_{11}$ & $<S_{21}$ for cross-sectional filled with high lossy material

For high lossy and fully loaded object, the errors for the proposed method are increased. The error in $|S_{11}|$ for PCTD is increased to 0.23% at lowest frequency and 1.3% for highest frequency. Error for RCTD is 1.75% and 4.61% for lowest and highest frequencies, respectievly. As expected, due to the insufficiency of RCTD for higher modes analysis, results for high lossy case is worser as to lossy and lossless cases. Again, the results for MoM with PCTD gives high accuracy for high lossy case, as to MoM with RCTD and HFSS.

For partially loaded objects, firstly a setup is prepared with three-layered lossless dielectrics. The relative permittivities of the layers are 6, 8 and 4, respectively. The object is cylindrical shaped and concentric with the waveguide. The radius of the object is equal to half of the waveguide. MMM could not be used for comparison. Also phase of S_{21} is not valid for HFSS. Amplitude and phase of S parameter results for half-loaded, three-layered, lossless dielectric object are given with Figure 3.7 and Figure 3.8 respectively.

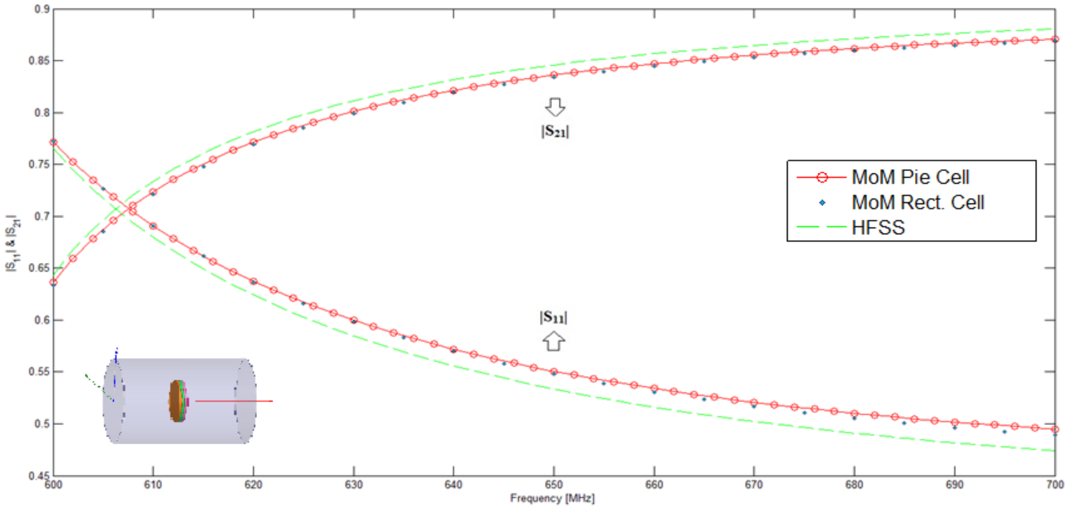

Figure 3.7 Comparison of $|S_{11}|$ & $|S_{21}|$ for half loaded with lossless material

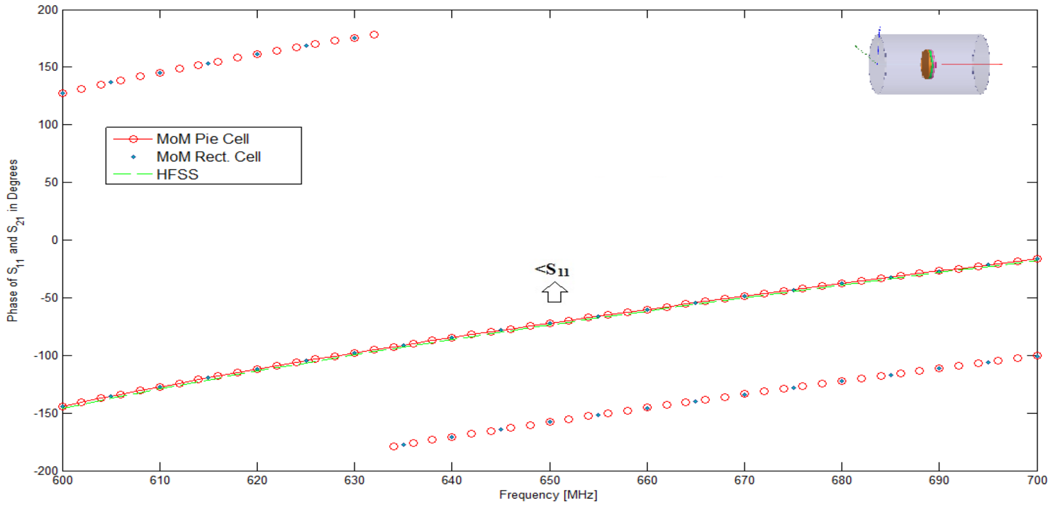

Figure 3.8 Comparison of $<S_{11}$ & $<S_{21}$ for half loaded with lossless material

For partially loaded object, MoM with PCTD, RCTD and HFSS is compared with each other. For lossless case, the differences in $|S_{11}|$ between PCTD and RCTD are 0.0647% and 1.1922% for lowest and highest frequencies, respectively. For $|S_{11}|$, HFSS follows PCTD with differences 0.85% and 4.1625% for lowest and highest frequencies, respectively.

The half-loaded object, mentioned above, is treated as a lossy structure in addition. Each layer has a complex part, $\varepsilon'' = \sigma / \omega\varepsilon_0$. To obtain a loss tangent around 0.001, the conductivities of materials are chosen as 2,55x10^{-4} *(S/m)*, 3,55x10^{-4} *(S/m)*, 1,55x10^{-4} *(S/m)*, respectively. Amplitude and phase of S_{11} and S_{21} parameters for half loaded, lossy model are shown in Figure 3.9 and Figure 3.10 respectively.

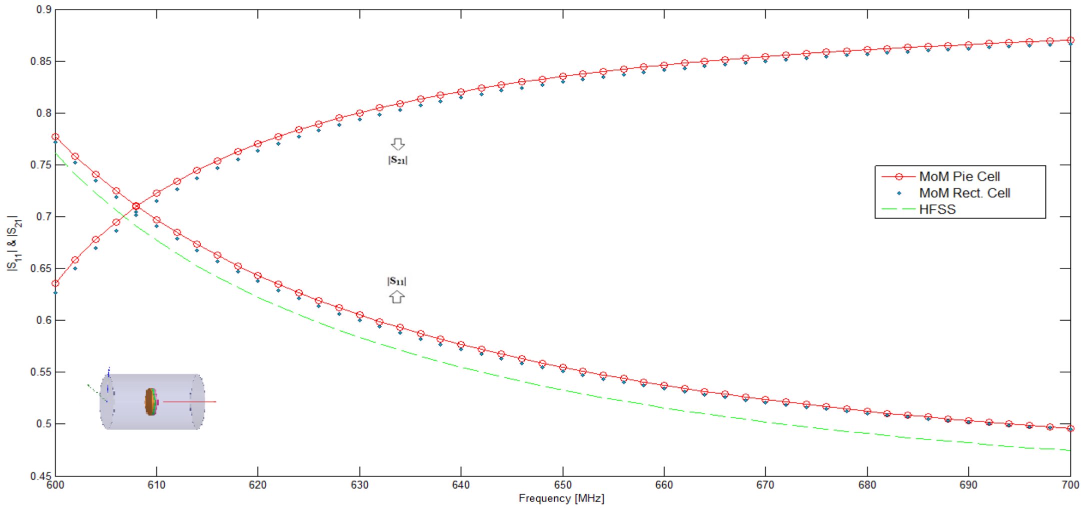

Figure 3.9 Comparison of $|S_{11}|$ & $|S_{21}|$ for half loaded with lossly material

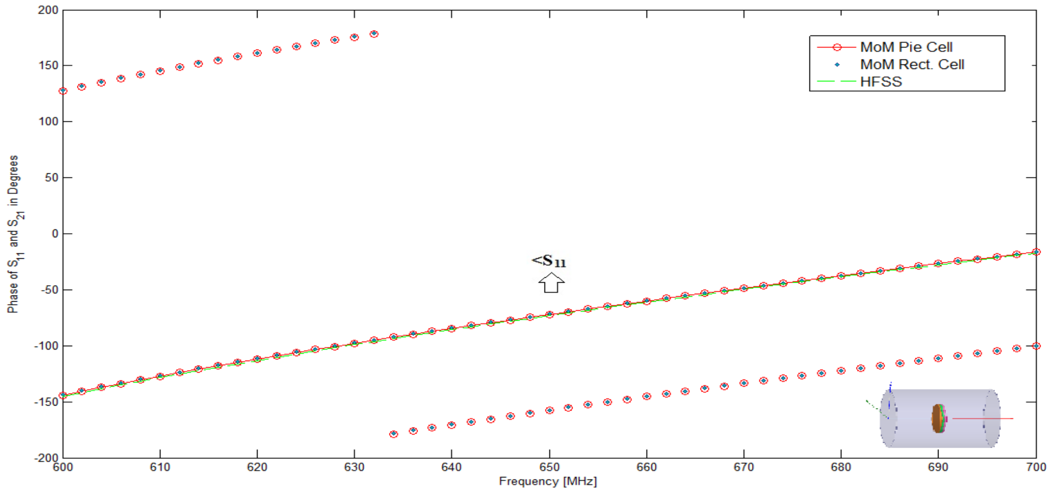

Figure 3.10 Comparison of $<S_{11}$ & $<S_{21}$ for half loaded with lossy material

Adding a loss to half loaded object caused PCTD and RCTD to follow each other with a little amount of difference. As to fully loaded case, difference between PCTD and RCTD for lossy case is not much. The number of modes, produced by the discountinity is less for half-loaded case as to fully loaded case. Also, since the size of the object is smaller, the cell size are decreased for half-loaded case. Hence, adding a loss, affected the consistency of RCTD less for half loaded case.

4. CONCLUSIONS AND RECOMMENDATIONS

In this study, analysis of arbitrarily shaped lossy dielectric materials loaded in circular waveguide is considered via an integral equation based MoM, which requires a dyadic Green's function representation as the kernel. In order to convert the vectorial integral equation into a system of linear equations, the object is divided into rectangular type cells, where the required integration of dyadic Green's function do not converge if observation and source points are at the same cell. Hence, a pie cell type divison is also proposed. Evaluation of integration of DGF at both cell types is introduced and discretization for MoM prodecure is explained in detail.

MoM and Mode Matching Method are used for the solution of the direct problem and validity of these methods is shown by numerical examples. The commercial software, HFSS, is also used for numerical comparisons. Since the ability of HFSS in circular geometries is not sufficient, satisfactory results could not be obtained. Nevertheless, for partially loaded materials, HFSS can be used as a bound reference.

It is observed through the numerical applications that optimization for Pie Cell Type Division (PCTD) is provided by increasing the cell number surrounding the center of the circular cross section. In order not to increase the computational load, simulations presented in this study are produced with 7 or 8 cells around the center, at most. This distrubiton enables the increment in ρ direction to be equal to that of ϕ direction. Meshing is generally done with cell dimensions around $\lambda/25$. In numerical results section, cell size in z direction is decreased to $\lambda/50$. Due to the computational efficiency of computer, one could not decrease the cell dimensions much more.

The evaluation of dyadic Green's functions is realized in this study. Errors, causing from numerical restrictions, can be tolerated with more powerful computer aid. The mesh structure for better accuracy is developed. A mesh structure with equal increment in ρ and ϕ directions is better for both computational load and calculation accuracy. Integration of Bessel functions, in the DGF expansion requires sensitive calculations, which increases the computational load.

4.1 Recommendations

This study is a basis for inverse algortihms to reconstruct the complex constitutive parameters of materials, using waveguide method. Evaluation of DGF for circular waveguide is determined. One can apply inverse algorithms for circular waveguide. Furthermore, validation of inverse algorithms for circular waveguide can be enabled with measurement data.

REFERENCES

[1] **Tie Jun Cui; Chang Hong Liang; Wiesbeck, W.** (1997). Closed-form solutions for one-dimensional inhomogeneous anisotropic medium in a special case. I. Direct scattering problem," *Antennas and Propagation, IEEE Transactions on* , vol.45, no.6, pp.936-941, Jun.

[2] **Golden, K.M.; Cheney, M.; Kung-Hau Ding; Fung, A.K.; Grenfell, T.C.; Isaacson, D.; Jin Au Kong; Nghiem, S.V.; Sylvester, J.; Winebrenner, P.;,** (1998). Forward electromagnetic scattering models for sea ice, *Geoscience and Remote Sensing, IEEE Transactions on* , vol.36, no.5, pp.1655-1674, Sep.

[3] **Philippe, A.; ,** (1973). Reflection and transmission of radio waves at a dielectric slab with variable permittivity, *Antennas and Propagation, IEEE Transactions on* , vol.21, no.2, pp. 234- 236, Mar.

[4] **Chun Chen; ,** (1978). An integral equation formulation of the direct scattering problem for an inhomogeneous slab, *Antennas and Propagation, IEEE Transactions on* , vol.26, no.6, pp. 797- 800, Nov.

[5] **J. R. Wait; ,** (1996). *Electromagnetic Waves in Stratified Media*. Institute of Electrical and Electronics Engineers, Oxford University Press, New York,. ch 3,4.

[6] **Jaggard, D. and Frangos, P; ,** (1987). The electromagnetic inverse scattering problem for layered dispersionless dielectrics. *IEEE Transactions on Antennas and Propagation*, Vol. AP-35.

[7] **Casey, K.; ,** (1973). Radiation from a line source near an inhomogeneous layer, *Antennas and Propagation, IEEE Transactions on* , vol.21, no.5, pp. 640- 648, Sep.

[8] **Peterson, A. F., Ray S. L. and Mittra R; ,** (1998). Computational Methods for Electromagnetics. New York, IEEE Press.

[9] **Wang. J. H.; ,** (1978). Analysis of a three dimensional arbitrarily shaped dielectric or biological body inside a rectangular waveguide, *IEEE Trans. Microw. Theory Tech,* **26**, 457-462.

[10] **Klymko, V.A.; Eshrah, I.A.; Yakovlev, A.B.; Kishk, A.A.; Glisson, A.W.; ,** (2004). Scattering by open metal obstacles in a circular waveguide: dyadic Green's function approach, *Antennas and Propagation Society International Symposium, 2004. IEEE* , vol.2, no., pp. 2127- 2130 Vol.2, 20-25 June

[11] **Akleman, F.; ,** (2008). Reconstruction of Complex Permittivity of a Longitudinally Inhomogeneous Material Loaded in a Rectangular Waveguide, *Microwave and Wireless Components Letters, IEEE* , vol.18, no.3, pp.158-160, March

[12] **Kilic, E.; Akleman, F. Esen, B. Ozaltin, D.M. Ozdemir, O. Yapar, A.; ,** (2010). 3-D Imaging of Inhomogeneous Materials Loaded in a Rectangular Waveguide, *Microwave Theory and Techniques, IEEE Transactions* on , vol.58, no.5, pp.1290-1296, May

[13] **Yaghjian, A.D.; ,** (1980). Electric dyadic Green's functions in the source region, *Proceedings of the IEEE* , vol.68, no.2, pp. 248- 263, Feb.

[14] **Balanis, C. A.; ,** (1989). Advanced Engineering Electromagnetics, John Wiley & Sons Inc., New York

[15] **Tai, C. T.; ,** (1994). Dyadic Green's Functions in Electroamgnetic Theory, Intext Educational Publishers, New York.

[16] **J. van Bladel.; ,** (1991). Singular Electromagnetic Fields and Sources. Oxford: Clarendon, ch 3.

[17] **Kun-Mu Chen.; ,** (1977). A simple physical picture of tensor Green's function in source region, *Proceedings of the IEEE* , vol.65, no.8, pp. 1202-1204, Aug.

[18] **M.Abramowitz and I. A. Stegun.; ,** (1972). *Handbook of Mathematical Functions with Formulas, Graphs and Tables.* Newyork. Dover Publications.

[19] **I. S. Gradshteyn and I. W. Ryzhik.; ,** (1965). Table of Integrals, Series and ing Experiment Station, Georgia Institute of Technology, Jan.Products. New York: Academic Press, ch 5.

APPENDICES

APPENDIX A.1: Analytical expression for $\int_0^z xJ_n(\lambda x)dx$

APPENDIX A.2: Analytical expressions for $\int_0^z J_n(\lambda x)dx$ and $\int_0^z xJ_n'(\lambda x)dx$

Appendix A.1

Analytical expression for $\int_0^z xJ_n(\lambda x)dx$

$$\int_0^z x^m J_n(x)dx = \frac{z^m \Gamma(\frac{n+m+1}{2})}{\Gamma(\frac{n-m+1}{2})} \sum_{k=0}^{\infty} \frac{(n+2k+1)\Gamma(\frac{n-m+1}{2}+k)}{\Gamma(\frac{n+m+3}{2}+k)} J_{n+2k+1}(z), \ [18]$$

where $\Re(n+m+1)>0$ **(A1.1)**

Due to the fact that the parameter of Bessel function is type of λx, one should apply change of variables. On the other hand, in this work, *m* is equal to 1. After some algebra, one obtains;

$$\int_0^{z'} xJ_n(\lambda x)dx = \frac{1}{\lambda^2}\left[\frac{z'\Gamma(\frac{n+2}{2})}{\Gamma(\frac{n}{2})} \sum_{k=0}^{\infty} \frac{(n+2k+1)\Gamma(\frac{n}{2}+k)}{\Gamma(\frac{n+4}{2}+k)} J_{n+2k+1}(z')\right], \ z'=\lambda z \quad \textbf{(A1.2)}$$

For a more compact expression and ease of computation , one can simplfy formula, using;

$$\Gamma(n+\frac{1}{2}) = \frac{1.3.5.7...(2n-1)}{2^n}\Gamma(\frac{1}{2}), \text{ where } \Gamma(\frac{1}{2}) = \pi^{\frac{1}{2}} \ [18] \quad \textbf{(A1.3)}$$

Arranging terms, one obtains;

$$\frac{\Gamma(\frac{n+2}{2})}{\Gamma(\frac{n}{2})} = \frac{\Gamma(\frac{n}{2}+1)}{\Gamma(\frac{n}{2})} = \frac{\frac{1.3.5.7...(2(\frac{n+1}{2})-1)}{2^{(n+1)/2}}\Gamma(\frac{1}{2})}{\frac{1.3.5.7...(2(\frac{n-1}{2})-1)}{2^{(n-1)/2}}\Gamma(\frac{1}{2})} = \frac{n}{2} \quad \textbf{(A1.4)}$$

Similarly;

$$\frac{\Gamma(\frac{n}{2}+k)}{\Gamma(\frac{n+4}{2}+k)} = \frac{4}{(n+2k+2)(n+2k)} \quad \textbf{(A1.5)}$$

Substituting (A.4) and.(A.5) into.(A.2), final expression of integral is given below;

$$\int_0^z xJ_n(\lambda x)dx = \frac{z'}{\lambda^2}\left[\frac{n}{2}\sum_{k=0}^{\infty} \frac{4(n+2k+1)}{(n+2k+2)(n+2k)} J_{n+2k+1}(z')\right], z'=\lambda z. \quad \textbf{(A1.6)}$$

This expression costs computation load for higher values of z'. For that reason, another analytical expression can be represented. Using the derivative of bessel function

$$J_n'(\lambda x) = \lambda[\frac{n}{\lambda x} J_n(\lambda x) - J_{n+1}(\lambda x)] \qquad \textbf{(A1.7)}$$

and compensate (C.1) with the formula, putting (A.7)

$$\int_0^z xJ_n'(\lambda x)dx = \frac{1}{\lambda}[zJ_n(\lambda z) - \int_0^z J_n(\lambda x)dx]$$

$$= \int_0^z x\lambda[\frac{n}{\lambda x} J_n(\lambda x) - J_{n+1}(\lambda x)]dx$$

$$= \int_0^z [nJ_n(\lambda x) - x\lambda J_{n+1}(\lambda x)]dx$$

Using some algebra, arranging the terms, one obtains the equality

$$\int_0^z xJ_{n+1}(\lambda x)dx = \frac{1}{\lambda}[(n+1)\int_0^z J_n(\lambda x)dx - \frac{z}{\lambda} J_n(\lambda z)] \qquad \textbf{(A1.8)}$$

For a more compact expression, letting $n=(n-1)$ in (A.8), one obtains;

$$\int_0^z xJ_n(\lambda x)dx = \frac{1}{\lambda}[(n\int_0^z J_{n-1}(\lambda x)dx - \frac{z}{\lambda} J_{n-1}(\lambda z)] \qquad \textbf{(A1.9)}$$

This is a new representation for $\int_0^z xJ_n(\lambda x)dx$ and consistent with the special case for $n=0$ given in [19]

Appendix A.2

Analytical expressiosn for $\int_0^z J_n(\lambda x)dx$ and $\int_0^z xJ_n'(\lambda x)dx$

Using recurrance relations [18]

$$\int_0^z J_{2n}(x)dx = \int_0^z J_0(x)dx - 2\sum_{k=0}^{n-1} J_{2k+1}(z), \qquad \textbf{(A2.1)}$$

$$\int_0^z J_{2n+1}(x)dx = 1 - J_0(z) - 2\sum_{k=1}^{n} J_{2k}(z) \qquad \textbf{(A2.2)}$$

and analytical expression for integral of 1st and 0th orders of bessel functions are

$$\int_0^z J_1(x)dx = 1 - J_0(z) \qquad \textbf{(A2.3)}$$

$$\int_0^z J_0(x)dx = zJ_0(z) + \frac{1}{2}\pi z\left[H_0(z)J_1(z) - H_1(z)J_0(z)\right] \qquad \textbf{(A2.4)}$$

,where $H_0(x)$ and $H_1(x)$ are the 0^{th} and 1^{st} orders of struve function and defined in power series expansion as

$$H_0(x) = \frac{2}{\pi}\left[z - \frac{z^3}{1^2.3^2} + \frac{z^5}{1^2.3^2.5^2} - \cdots\right] \qquad \textbf{(A2.5)}$$

$$H_1(x) = \frac{2}{\pi}\left[\frac{z^2}{1^2.3} - \frac{z^4}{1^2.3^2.5} + \frac{z^6}{1^2.3^2.5^2.7} - \cdots\right] \qquad \textbf{(A2.6)}$$

one can derive the analytical expression for the integral of $\int_0^z J_n(\lambda x)dx$

The expression (A2.4) may cost time requirement and computation load for higher values of z. For that reason, on emay use analytical expression for integral of any order bessel function including infinite sum, namely;

$$\int_0^z J_n(x)dx = 2\sum_{k=0}^{\infty} J_{2k+n+1}(z) \quad \textbf{(A2.7)}$$

which can be controlled numerically, whether converged or not.

It should be noted that, in this work, the parameter of bessel function takes the form of "*λx*" or "*μx*"instead of "*x*". Hence, deriving the proper expressions, one should apply change of variables. After some algebra, letting the parameter of bessel function *"λx"*, arbitrarily, one can obtain;

$$\int_0^z J_n(\lambda x)dx = \left\{ \begin{array}{ll} zJ_0(z') + \frac{1}{2}\pi z\left[H_0(z')J_1(z') - H_1(z')J_0(z')\right] \text{ or } \frac{2}{\lambda}\sum_{k=0}^{\infty} J_{2k+n+1}(z') & \text{n=0,} \\ \frac{1}{\lambda}[1 - J_0(z')], & \text{n=1,} \\ \frac{1}{\lambda}[\int_0^{z'} J_0(x)dx - 2\sum_{k=0}^{\frac{n}{2}-1} J_{2k+1}(z')], & \text{n is even,} \\ \frac{1}{\lambda}[1 - J_0(z') - 2\sum_{k=1}^{\frac{n-1}{2}} J_{2k}(z')], & \text{n is odd} \end{array} \right\} \quad \textbf{(A2.8)}$$

where $z' = \lambda z$.

Analytical expression for $\int_0^z xJ_n'(\lambda x)dx$

Using integration by parts, $u = x,$ $\mathrm{d}v = J_n'(\lambda x)dx$ and $du = dx,$ $v = \frac{1}{\lambda}J_n(\lambda x)$, one can derive $\int_0^z xJ_n'(\lambda x)dx = \frac{1}{\lambda}[zJ_n(\lambda z) - \int_0^z J_n(\lambda x)dx]$ **(A2.9)**

CURRICULUM VITAE

Name Surname:	Ahmet Aydoğan
Place and Date of Birth:	Mardin 11/06/1987
Address:	Mecidiyeköy Mah. Dereboyu Cad. 33/1 Şişli/İstanbul
E-Mail:	ahmetaydogan87@gmail.com
B.Sc.:	Istanbul Techical University, Electronics and Communication Engineering Department, Telecommunication Engineering programme.